DR 2.2: Intelligent Shared control for navigation and mobile manipulation

Petter Ögren[*], Mario Gianni[†], Hartmut Surmann, Rainer Worst[‡], Michael Achtelik[§], Renaud Dubé, Abel Gawel[¶] and the TRADR Consortium

[*]*KTH - Royal Institute of Technology, Stockholm, Sweden*
[†]*University of Rome - Alcor Lab, Rome, Italy*
[‡]*Fraunhofer IAIS, Sankt Augustin, Germany*
[§]*Ascending Technologies GmbH, Krailing, Germany*
[¶]*ETH Zürich - Autonomous Systems Lab, Zurich, Switzerland*
⟨`petter@kth.se`⟩

Project, project Id:	EU FP7 TRADR / ICT-60963
Project start date:	Nov 1 2013 (50 months)
Due date of deliverable:	Month 26
Actual submission date:	15th of February 2016
Lead partner:	KTH
Revision:	final
Dissemination level:	PU

This document describes the work of providing the TRADR robots with motion capabilities in modes where the control is shared between the operators and the robots. For the UGV we have developed and tested a new control interface inspired by computer games and a Bayesian non-parametric approach learning patterns of control maneuvers. We have also developed a new mapping/planning framework, where planned paths do not have to be recomputed from scratch every time the map is updated with new information. In addition, a Mixed-initiative approach for path planning has been used to improve scalability, allowing the user to add waypoints and knowledge about the reachability of those waypoints into the planner. For the UAV we have developed indoor capabilities, in terms of localization in GPS denied areas, and obstacle avoidance in terms of virtual bumpers.

Executive Summary

This report describes work towards providing the TRADR robots, Unmanned Aerial Vehicles (UAVs) and Unmanned Ground Vehicles (UGVs) with motion capabilities, in terms of intelligent shared control for navigation and mobile manipulation.

Formally, the report constitutes deliverable (D2.2), the second year deliverable of WP2 (persistent models for acting). The aim of WP2 is to endow the TRADR robots with motion capabilities. During the second year, WP2 included tasks T2.2 (Intelligent teleoperation for mobile manipulation) and T2.5 (Shared navigation) and targets milestone MS2.2 (Intelligent Shared Control for Navigation and Mobile Manipulation).

In task T2.2 (Intelligent teleoperation for mobile manipulation) the UGV was endowed with a new control mode inspired by computer games. This control mode was shown in user studies to outperform the classical teleoperation control mode in both search and navigation tasks. The new control mode was also extended with a component that allowed the user to assess the current network connectivity situation and take that information into account, while still focusing on the primary objective of exploring an environment.

Task T2.5 (Shared navigation) involved both the UGVs and the UAVs. For the UGVs, we developed a new mapping/planning framework, where planned paths do not have to be recomputed from scratch every time the map is updated with new information. We also improved scalability of the planner using a Mixed-initiative approach, allowing the user to add waypoints and knowledge about the reachability of those waypoints into the planner. Furthermore, a Bayesian non-parametric approach, based on the Dirichlet Process-Gaussian Process (DP-GP) mixtures, has been proposed to learn patterns of control maneuvers for the UGV.

For the UAV we have developed indoor capabilities, in terms of localization in GPS denied areas, and obstacle avoidance in terms of virtual bumpers. Continuously exploring several options, we are evaluating a high performance combination of structured light and stereo, provided by Intel, in possible combination with ultrasonic sensors, laser height sensors, as well as a low cost option using only omnidirectional vision.

Role of intelligent shared control for navigation and mobile manipulation in TRADR

Mobility of the TRADR robots is of key importance to the successful execution of the disaster response scenarios. In many instances, the overall system performance is improved when both operator and robot can contribute with their key strengths. This is the focus area of intelligent shared control.

Contribution to the TRADR scenarios and prototypes

The motion capabilities of the TRADR UAVs and UGVs are essential for the use cases. In particular, the content of this deliverable relates to the following use cases (see deliverable D7.2):

- Generic use case 1: *UAV[x] detect/search for X, using method Y* Capabilities for this use case are described in Section 1.5 below.
- Generic use case 3: *UGV[x] go to location X (optionally via Y).* Capabilities for this use case are described in Section 1.3 below.
- Generic use case 4: *UGV[x] go to location X on (semi)autonomous mode.* Capabilities for this use case are described in Section 1.4 below.
- Generic use case 5:*UGV[x] detect/search for X, using method Y.* Capabilities for this use case are described in Section 1.3 below.
- Generic use case 6: *UGV[x] manipulates object X* Capabilities for this use case are under current developments, but not included in this deliverable.
- Generic use case 7: *UGV[x] encounters obstacle X, takes action Y to overcome* Capabilities for this use case are described in Section 1.3 1.4 below.
- Generic use case 8: *UGV[x] avoids colliding with actor X* Capabilities for this use case are described in Section 1.3 and 1.4 below.

Persistence

The actions in WP2 are, and will be, persistent in the following way. First, the path planning is integrated with the persistent maps, allowing a planned, and/or executed path to be saved and reused, in spite of the map being updated/refined with new information, furthermore, maps that were analyzed for traversability and saved in one sortie can be reused in a following sortie without the need for re-processing. Second, persistence will be achieved by working across levels of autonomy. When executing tasks such as traversing difficult terrain, or grasping an object in intelligent teleoperation mode, the system will save parts of the state trajectories, and then reuse those when performing actions in full autonomous mode. Thus improving performance across sorties.

1 Tasks, objectives, results

1.1 Planned work

The work described in this report (D2.2) was performed within the scope of Tasks T2.2 (Intelligent teleoperation for mobile manipulation) and T2.5 (Shared navigation), targeting the milestone MS2.2 (Intelligent Shared Control for Navigation and Mobile Manipulation). The objectives of these tasks were given as follows:

- *The goal of Task 2.2 is to develop an Intelligent teleoperation mode for mobile manipulation. In such a mode the user is constantly interacting with the UGV, but an intermediate control layer is reducing work load and improving situational awareness throughout the execution.*
- *The goal of Task 2.5 is to develop new models for shared operation of both UGVs and UAVs. Full teleoperation requires the human operator to provide commands for all actuated degrees of freedom, which, in the case of the UGV is difficult due to the four flippers. On the other hand, complete autonomy prevents the operator from using any command. Task 2.5 aims at finding a balance between those two opposites. One outcome could be to allow humans to modify online a path computed by the path-planner, and to introduces dynamic maps into the robots' path-planning considerations.*

1.2 Addressing reviewers' comments

Below we collect the reviewer comments made regarding WP2, with corresponding answers.

1. The interdependencies and even redundancy between different WPs should be addressed more carefully and more clearly, especially between WP1 and WP2 (path-planning algorithms), between WP4 and WP5, and between WP3 and WP7. There is a need for better coordination and more intensive joint research work between the respective partners.

   Response: The path planner is now the sole responsibility of Roma, and will be reported in WP2.

2. The excessive planning time issue should be more deeply investigated to determine its main causes and modify the system with the aim of mitigating the phenomenon.

   Response: Two main causes actually affect the path planning performance, namely, the computational time needed to compute the representation of the environment on top of which planning performs its own reasoning, and the dimensionality of the search space of the path planning algorithm. In order to cope with these issues, way-point selection has been considered. Way-points are provided by the human operator through a suitable interface, as preferences of where the robot should go. Pairs of way-points can then be given as input to the path planning algorithm. The distance between two consecutive way-points is expected to be shorter than the distance between the first and the last selected way-point. This implies that the algorithm can compute path segments of short distances, rather than an entire long distance path. For such a computation the planner needs only a portion of the entire representation of the environment, namely that part comprising the pair of way-points under consideration. This approach can reduce the size of the search space, thus enhancing the path planning performance, see Section 1.4.3 below.

3. There seems to be some room for improvement in the design of the UGV with flippers and arm and external sensors (e.g. less obstruction of laser scanner's field of view).

   Response: It is too late to change the robot construction. We note that the design is a compromise. For practical handling reasons the robot should be as compact as possible, which naturally contradicts the sensory placement which needs to be dispersed to avoid occlusion.

4. The integration team is reporting continued frustration over wifi/networking failures. There is no infrastructure to support this that can be easily bought as COTS components. And in fact this is likely to occur in any realistic scenario. Given this, they need to make sure all WPs produce contributions that can work with bad connections. All WPs should show network resilience to degradation in quality of connection, and the integration team should test for it, report on it, etc.

   Response: We have started investigating how to include network connectivity awareness into the intelligent teleoperation mode of T2.2, see Section 1.3 below.

The work performed in the areas of intelligent shared control of UGV and UAV is presented below.

1.3 Task 2.2 Intelligent Teleoperation of UGVs

In many UGV teleoperation missions, the *time* needed to complete a mission is critical. Victims in burning houses can be saved, a bomb on a timer can be dismantled, and in military operations, staying too long in the same place is a risk in itself [1],[2]. A number of studies have been performed to investigate how the mission time is divided between different activities [1, 3, 4, 5, 6], and a well established conclusion is that a significant amount of the time is spent creating and maintaining the *situational awareness* of the operator. In fact, the fraction of mission time spent on improving situational awareness was estimated to as much as 49% in [5] and to roughly 30% in [6]. Furthermore, [7] concluded that most of the critical incidents in the investigated Urban Search And Rescue (USAR) competition was due to lacking situation awareness. The things that make situational awareness difficult for the operator is the high cognitive workload, in combination with poor lightning conditions and narrow fields of view, which makes it hard to for the operator to estimate scales using a video stream, [4].

In this project, we continue along the lines suggested in [8, 9, 10] and draw inspiration from the computer game industry in the design of the UGV control interface. In particular, we turn our attention to the so-called First Person Shooter (FPS) genre, including titles such as Quake, Doom, Halo, Half-Life, and Call of Duty [11, 12]. There are interesting correspondences between the task requirements of teleoperated FPS-agents and USAR-UGVs. In both situations, a human operator is to control an entity, using a video screen and an input device such as a game pad, that is to complete a task by moving around in a 3D environment, often switching between searching and navigating.

There are several reasons to think that the FPS control mode, also known as *Free Look Control* (FLC)[1] is good for teleoperation.

First, in FLC *Translation* and *Rotation* are decoupled. That is, translation is controlled with one device (joystick 1 or the keyboard) while rotation is controlled with another device (joystick 2 or the mouse). This makes it easy to point the camera in the desired direction reducing the amount of attention needed to control the UGV, thus leaving more cognitive capacity for the surroundings of the UGV. On the other hand, in *Tank Control*, that is used in most UGV systems today, the input devices (sticks) are assigned to different parts of the UGV hardware. One stick controls the UGV tracks, moving forwards/backwards, or rotating right/left, while the other stick controls the pan/tilt-unit, panning right/left or up/down. This creates a redundancy in rotation, both pan/tilt and tracks can produce rotation, while translation sideways has to be achieved by a rotate-translate-rotate sequence.

Second, the developments in the computer game community gives a clear indication that human operators prefer FLC to Tank Control. The first successful FPS games are considered to be Wolfenstein 3D and Doom [11], which appeared in 1993. Both these used Tank Control, which was standard in the genre until 1996 when the game Quake was released. In Quake, there was an option to use another control mode, FLC, and in 1997, with Quake 2, the FLC option was made the default choice [12]. Since then, FLC has totally dominated the genre, with a few notable exceptions, that actually provide additional arguments for using FLC. *Resident Evil* is one of the

[1] *Free Look Control* is also sometimes called *Mouse Look Control*.

few games still using Tank Control, and when asked to explain the reasons why, the producer, Jun Takeuchi, answered as follows: "I think that by imposing certain restrictions on the player you actually help to heighten the fear and the tension, and, ultimately, you create a better horror game." [13]. Thus, in the gaming community, Tank Control is known to heighten the fear and the tension of the user, which makes it highly inappropriate for UGV teleoperation, given the situational awareness problems described above.

Third, even if the two control modes were equally efficient, it would still make sense to control UGVs in the same way as the majority of the computer games, in order to take advantage of the number of pre-trained operators available. In fact, as noted by Gkikas et al. "There is a large existing expert player community that has developed sensorimotor skills comparable to these of a musical instrument player or an expert typewriter. Actually, one important aspect of game satisfaction for these people is the challenge of achieving mastery in these skills" [11].

In a typical search and rescue task, the UGV operator switches between navigating (following a known path to get to a given location) and exploration (searching an area for objects or victims). We wanted to test the two control modes in both these scenarios. Therefore, we created a virtual environment with two instances of a path following scenario, such as the one in Figure 1 and two instances of an exploration scenario, such as the one in Figure 2.

Figure 1: In the path following scenario, the operators should follow the dashed path, while avoiding collisions with moving and static objects, and reach the end in minimum time.

To compare the two approaches we performed a user study with 16 subjects. The outcome of the exploration scenario can be seen in Figure 3, with a clear performance increase for FLC.

The outcome of the path following scenario was also better when operators used FLC, as can be seen in Figure 4.

Figure 2: In the exploration scenario, the operators should search for marker symbols, such as the X on the wall to the left, and try to find as many as possible in 2 minutes time.

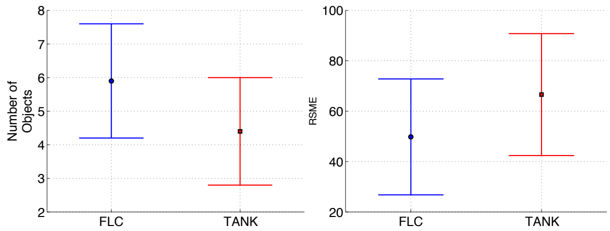

(a) (b)

Figure 3: In the Exploration scenario using FLC, more object were found (a), and a lower mental workload was reported (b).

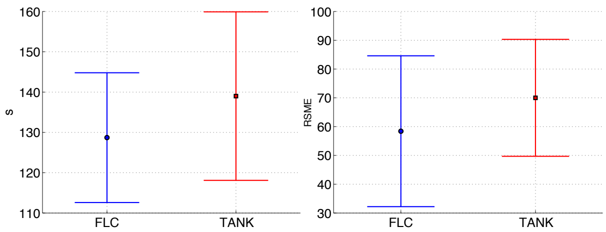

(a) (b)

Figure 4: In the Path following scenario using FLC, shorter mission times were measured (a), and less workload was reported (b).

A more qualitative sense of the advantages with FLC can be seen in Figure 5 and 6. There, the positions occupied by the UGVs throughout the 16 trials is seen in the two maps. As can be seen the operators using FLC were able to achieve a more evenly spread cover of the map, in particular of the northern most parts of Figure 5. More details on these results can be found in the Appendices, Section 2.1.

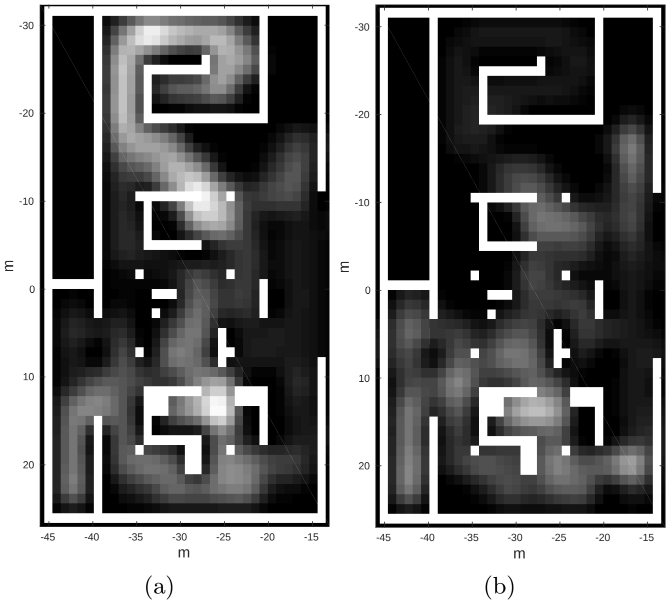

Figure 5: The most visited parts of the Exploration scenario (version 1) using FLC (a), and Tank Control (b).

During teleoperation, it is very important to maintain connectivity between the operator and the robot. Otherwise the robot will be stranded, or have to rely on autonomous fallback functionality to move back into an area with sufficiently good connectivity. As seen above, the situational awareness of the operator is a key parameter in mission performance. To improve mission performance during teleoperation it is therefore important to allow the operator to have a situation awareness that includes the network connectivity dimension, without reducing the spatial awareness.

We addressed this problem by a twofold approach. First we estimated the gradient of the Radio Signal Strength (RSS) at the robot position, then we communicated this gradient information in terms of a colored bar, around the video feed. This approach is illustrated in Figure 7.

For the approach above to be useful, we needed to test wether the RSS gradient predictions were stable and accurate enough to provide guidance to the robot operator. To do that we recorded RSS as well as RSS gradient estimates and robot velocities for a mission. In theory, the dot product between the gradient and the robot velocity should equal the time derivative of the RSS, but for the set up to be useful it is enough that they have the same sign, i.e. moving in the direction of the gradient estimate gives an

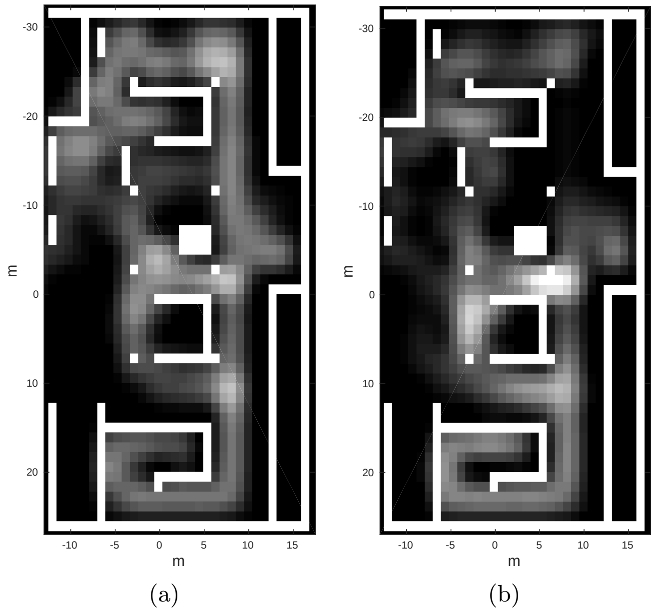

Figure 6: The most visited parts of the Exploration scenario (version 2) using FLC (a), and Tank Control (b).

increase in RSS and vice versa. Figure 8 shows that this is indeed the case. More details on these results can be found in the Appendices, Section 2.2.

1.4 Task 2.5 part 1: Shared Navigation of UGVs

This section introduces dynamic maps into the path-planning considerations. First the concept of the new graph-based mapping framework is briefly introduced, as opposed to the static mapper used at the beginning of the TRADR project. Then the interaction between planning and dynamic maps is elaborated. Finally we comment on practical experiences with the systems infield.

1.4.1 Dynamic mapping

In order to introduce the capability for dynamic maps, a new mapping framework was designed following the approach in [14]. The framework is based on a variant of graph-SLAM introducing continuous-time state corrections. A good overview of recent contributions in continuous-time state estimation can be found in [15]. The specific advantage of the approach is that it captures high-rate measurements with low state-space size by using composition states. These composition states are the union of static high-rate measurements and dynamic low-rate corrections, i.e. the robot trajectories. Using this concept we provide a mapping framework that stays dynamic over time

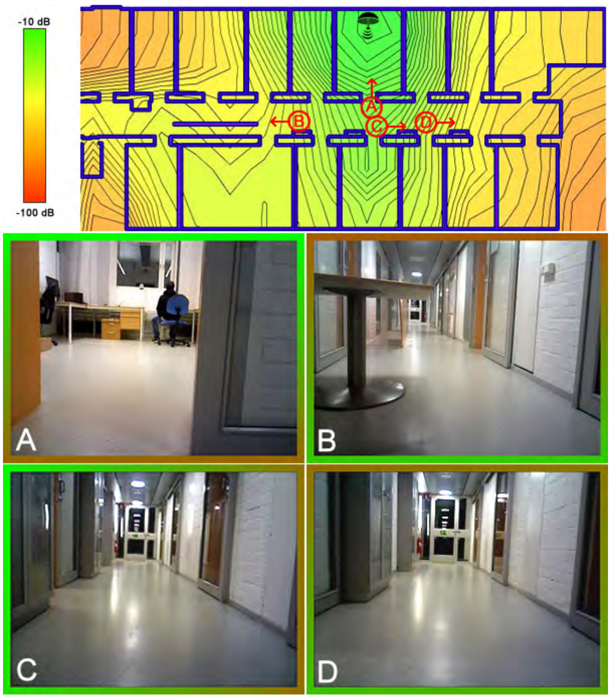

Figure 7: At the top we see the Radio Signal Strength over an indoor area, with the transmitter at the top middle, and four different robot poses, denoted by A, B, C and D. At the bottom we see the video feed of the corresponding robot poses, along with a color border indicating the gradient of the RSS (going from red to green).

and can potentially be used for very large persistent mapping over multiple sorties and by multiple robots. The nodes, i.e. the states of the graph-based map can arbitrarily be activated or deactivated for optimization as needed. Many sorts of mapping modules can be simply added as further constraints or information on individual nodes, e.g. loop-closures, object detections, traversability information. The graph structure ensures that the information within the map stays persistent and can be updated when new information is added to the graph.

1.4.2 Planning on dynamic maps

The graph structure enables the registration of planned paths relative to the nodes of the graph. Planned paths can therefore be locally registered to nodes and adapt with local changes to the map without the necessity for full replanning once map updates occur. Since the mapping and the path-planning module are still under concurrent development and not fully deployed on the TRADR systems, we use the intermediate solution of providing the point-cloud-based interface as previously employed with the static

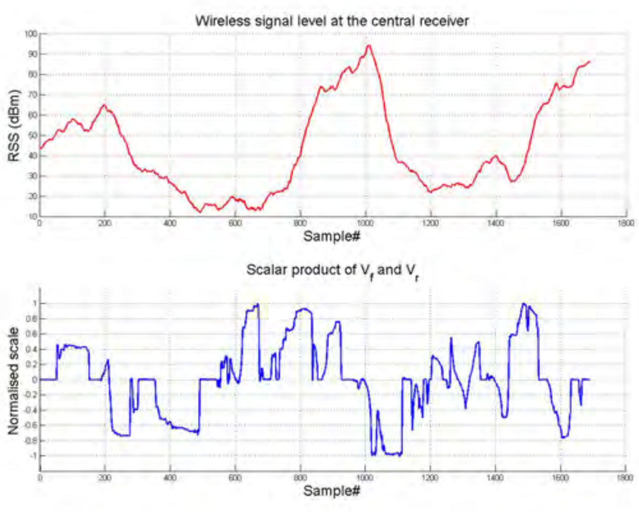

Figure 8: Theoretically, the time derivative of the RSS should equal the dot product between robot velocity and RSS gradient. As can be seen above, the sign of the blue curve (dot product) does capture the derivative of the red curve (RSS).

mapper. The maps are dynamically generated and updated, but the path planner cannot yet benefit from the local registration of paths. However, since the planner presented in 1.4.3 is capable of computing short path-segments between waypoints, this intermediate solution already provides planning on dynamic maps without full replanning of paths while the elegant final interface is pending completion.

During the TRADR joint exercise, we did several experiments with planning on maps which have been retrieved from previous experience. By providing an interface for storing and loading maps, persistence is possible across different sorties. The novel mapping techniques described in [D1.2] will support this same interface.

1.4.3 Mixed-initiative approaches for path planning

The TRADR joint exercise in Year 2 has highlighted a crucial problem of the 3D path planning algorithm that was used on the UGV platform, namely, scalability [16]. In order to compute a path toward a goal, the algorithm needs to reason on a semantic representation of the environment, built on top of the 3D metric map. This representation provides an estimate of the traversability cost of the surroundings [16, 17]. In order to be calculated, this cost requires a preliminary segmentation of the incoming point cloud as well as estimate of normals. The computational complexity of these operations turned out to grow exponentially as the size of the point cloud

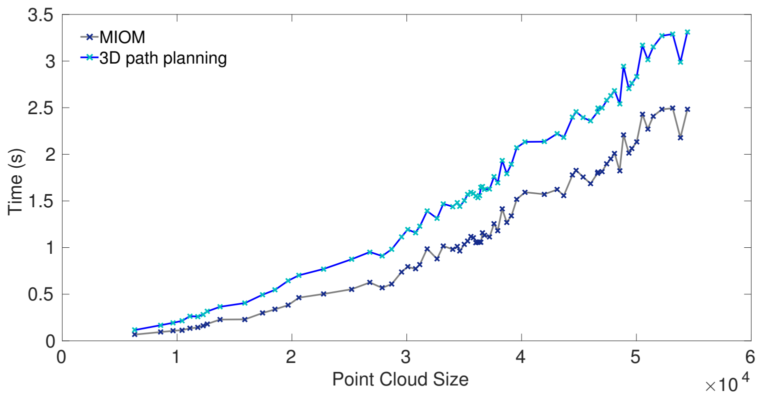

Figure 9: Computational cost, with respect to time, of path planning, with and without operator intervention through MIOM, as the size of the incoming point cloud increases. For $\sim$ 55 mln points, planning with way-point takes 2.482 sec. for computing a path, rather than 3.314 sec.

increased. Moreover, we observed during evaluation that for short-distance targets, posted by the operators, the path planning algorithm still computed safe paths according to traversability. This in-field experience suggested three main improvements in path planning to speed up computation. The first improvement resembles the mechanism of both storing and retrieving maps, described in the previous paragraph, to demand traversability analysis in batch processing. Under this processing, maps stored in previous sorties can be analyzed for traversability and then retrieved by the robot without the need to be re-processed before the start of a new sortie. Moreover, it allows the robot to run traversability estimates on demand, thus, batch processing can be scheduled when it is required rather than doing continuous updates of the traversability map. The second improvement concerns way-point navigation and knowledge integration. We implemented a Mixed-Initiative Operational Model (MIOM) which extends the reasoning capabilities of the robot, directly intervening on the state of both traversability mapping and path planning. The proposed model exhibits a set of actions which the operator can perform. Internally, the model maps such actions in events which directly affect robot computation. For example, the operator can insert, modify or delete waypoints on top of the traversability map. Different colors ranging from blue to red visually inform the operator of the degree of safety of a region regarding traversability. Given the way-point added by the operator, MIOM limits the search of the path to the section of the point cloud between consecutive points. Moreover, it modifies the estimate of the traversability cost of the points in the neighbourhood of a way-point with a scaling factor which captures the operator knowledge about reachability of that point. This update has the main advantage of enhancing the overall performance of path planning. Figure 9 shows that for the search of a path on a point cloud of size $\sim$ 55 mln points, 1.3352 sec. less are required for planning with waypoints.

MIOM has been implemented in the main TRADR Operator Control Unit (OCU) interface. For more details and results concerning this research work we refer to Section 2.4.

1.4.4 Motion patterns control learning of TRADR UGV

In order to explore a rescue scenario, the robot has to move through narrow passages, overcome obstacles, crawl over rubble, climb stairs, and follow paths along sandy terrains. These navigation tasks can be executed, through manual controls provided by an operator, in a semi-autonomous fashion through a controller which supports the operator in managing of a sub-set of commands, or under a full autonomous controller. Manual control is very demanding for a human operator, in particular when the remote visual feedback is not so accurate. Manual control is a source of stress and, very often, it causes the operator to lose control of the navigation task, resulting in a loss of situation awareness. Conversely, full autonomous control is often not robust enough to ensure safe navigation. Semi-autonomous control turns out to be a good trade-off between the workload of an operator and the accuracy of a fully autonomous controller. Nevertheless, an alternative solution might be to endow an autonomous controller with a set of strategies, and the capability to switch among these strategies in the case in which the robot has to negotiate rubble, rather than stairs, mud or sand.

Building such a strategy selector is a challenging task since it requires both a classification of all the kind of terrain surfaces which can be traversed by the robot and the development of a control strategy for each of these terrains. A preliminary solution to this complex problem is to learn a set of the control manoeuvres from a set of trajectories, previously tracked by the robot and enriched with the associated terrain features and the control commands used follow these trajectories. To this end, we proposed a Bayesian non-parametric approach to modeling the motion control of the TRADR UGV. The motion control model is based on a Dirichlet Process-Gaussian Process (DP-GP) mixture model [18, 19]. The DP-GP mixture model provides a flexible representation of patterns of control manoeuvres along trajectories of different lengths and discretizations. This representation allows us to group trajectories sharing either patterns of control manoeuvres or path segments. Finally, the model estimates the number of patterns, sufficient for modeling the dynamics of the UGV. Preliminary results on a data-set of 50 trajectories, collected in simulation, show that, after the estimation of the parameters of the DP-GP mixture model, 25 patterns have been segmented with an accuracy of 72.3%. Then, the model learnt a mixture of control strategies, together with the weights of each strategy. Given both a trajec-

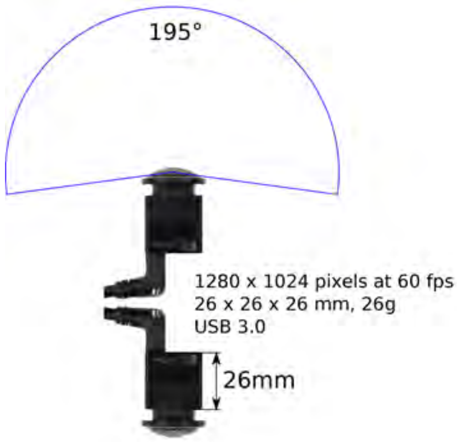

Figure 10: The UAV omnidirectional camera system

tory and a set of features, the hypothesis of the best control strategy which have to be applied for tracking this trajectory is derived through maximum a posteriori. More details about this work can be found in Section 2.5.

1.5 Task 2.5 part 2: Shared Navigation of UAVs

As for the UGV also the UAV has to navigate based on way points. This was implemented in year one by GPS waypoints, but navigation in GPS denied environments is still an open issue. The base for the navigation is the self localization of the UAV which is much more difficult in GPS denied environments. UAVs only have a very limited payload i.e. the selection of the sensor and computing equipment is very critical and limited by the weight. The following section describe our current approach for the self localization of the UAV in GPS denied environments, based on two omnidirectional cameras [20] (Annex Overview 2.3). An overview of state of the art techniques for localization of flying robots with a focus on optical cameras is given in the state of the art section of this document, see Section 1.6.

1.5.1 System design

The camera system for our localization approach is shown in Figure 10. The two cameras have extreme wide-angle lenses (195° fish eye lenses) and are mounted in opposite directions. The common pin hole camera model does not hold for such wide-angle lenses, instead the properties of this omnidirectional camera system can be modeled by the camera model described by Scaramuzza [21].

The developed localization approach is based on global appearance techniques i.e. it uses the hole image and not only single features. The basic requirement is the presence of reference images against which the position can be determined. The current position is estimated relative to the reference image. The localization procedure can be subdivide in the following five tasks:

1. Generate reference frames in the environment (i.e. get images from all locations, floors, rooms, ...).
2. Calculate image descriptors of the reference frames and save the descriptors in a data base.
3. Take test images at the current position.
4. Calculate images descriptors of the test images. (for comparison with the data base).
5. Compare the test image descriptor with the data base and find the nearest descriptor (i.e. with the minimal distance).

For the descriptors we used the Histograms of Oriented Gradients (HOG) of the omnidirectional images. Originally HOG are used to detect human contours [22], but Hofmeiter et al. also used it to localize ground robots [23]. The following section briefly describes the construction of HOG descriptors used for UAVs.

1.5.2 HOG descriptor

The first step of the calculation of a HOG descriptor of the two omnidirectional images is the generation of a panorama image. The periphery of a circle and the radius of an omnidirectional image are used as the width and height of the panorama image (see Fig. 11). The panorama image is used to calculated the gradients. Therefore the convolution with the following matrix is done:

$$D_x = [-1\ 0\ 1] \qquad D_y = [-1\ 0\ 1]^T$$

The resulting horizontal i_x and vertical i_y components of the pixel i are used for the calculation of the gradient $|G|$ and orientations Θ.

$$i_x = i * D_x \qquad i_y = i * D_y$$

$$|G| = \sqrt{i_x^2 + i_y^2} \qquad \Theta = atan2(i_y, i_x)$$

The magnitudes of each pixel are subdivided in two classes of orientations. The gradient orientation Θ is for example 43° and is between the class of 0° and 45°. The main part of the magnitude $|G|$ is assigned to the 45° class.

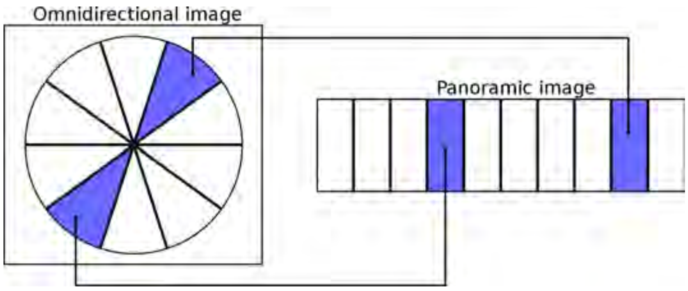

Figure 11: The relationship between the omnidirectional image and the panorama image.

A histogram can be calculated by distributing the magnitudes to orientation classes but we subdivide each image in several cells and calculate the histogram for each cell. The already distributed gradients are subdivided on its two next cells where the distance to the cell midpoints specifies the division factor. The subdivision of the image is done twice, even in horizontal and one more time in vertical cells, see [24, page 3044]. The result are two HOG vectors for an image.

The vertical HOG Vector, i.e. the sum of all vertical histograms is reduced by condensing of two opposite cells of the omnidirectional images. Figure 11 shows a blue marked cell pair. A further optimization is achieved by the combination of the vertical cells over both panoramic images (lower and upper camera). The horizontal cells can not be optimized while the vectors of both images are only concatenated. Thereafter, a vertical and a horizontal HOG vector represents a pair of two panoramic images.

The final HOG descriptors are generated by a normalization of the HOG vectors. The vectors are normalized in blocks, where one block includes three cells or histograms. So, each block has a cell together with its neighbors. The normalization of a block vector v is done with the L2-norm [22, page 6].

$$v \longrightarrow \frac{v}{\sqrt{(\|v\|_2)^2 + \epsilon^2}}$$

The value ϵ prevents a division by zero if images have no gradients. Usually it is $\epsilon = 1$. The euclidean norm $\|v\|_2$ is defined as:

$$\|v\|_2 = \sqrt{\sum_{i=1}^{n} |v_i|^2}$$

Figure 12 summarizes the descriptor generation. It shows the division into horizontal cells, the determination of the histograms and the grouping to a HOG descriptor.

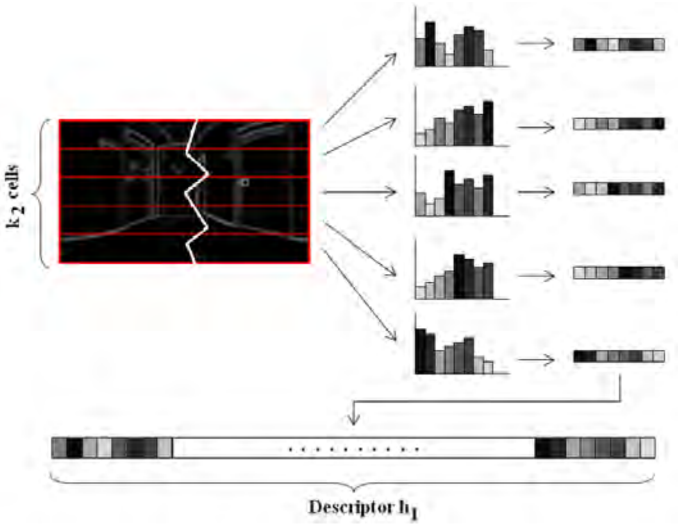

Figure 12: The schematic representation of the generation of an HOG descriptors without normalization [24, page 3044].

1.5.3 Evaluation

The first evaluation of the localization approach took place in the disused blast furnace plant Phoenix West at Dortmund-Hörde (Germany), during the second TRADR Joint Exercise from May 18th to May 22th in 2015.

Several times, the furnace plant was explored with the camera system and reference as well as test images were recorded. The first recording defines the references images and reference areas and the next recordings the test data for the HOG localization. The goal is to find the nearest references images from the given test images to localize the camera. For the evaluation we pre-assigned images to the right areas and thus offered the ability to detect a misallocation of HOG the localization process.

Figure 13 shows an example of the evaluation with two values for each area. The diagram will be explained referring to the first (*HalleB*) part. The first bar indicates how many images are localized directly at the area *HalleB* (with the highest value). The second bar indicates how many images are localized at the area *HalleB* under the top 5.

Figure 14 shows some sample images and examples for three different errors:

Similarities
Some areas of the hall look very similar, analog to corridors in office buildings. In our case the correct area is still in most cases among the five areas. The symmetrical construction of the blast furnace no. 5 is the reason for the poor results of the *HO5L*-area, because the images are assigned to the opposite field *HO5R*.

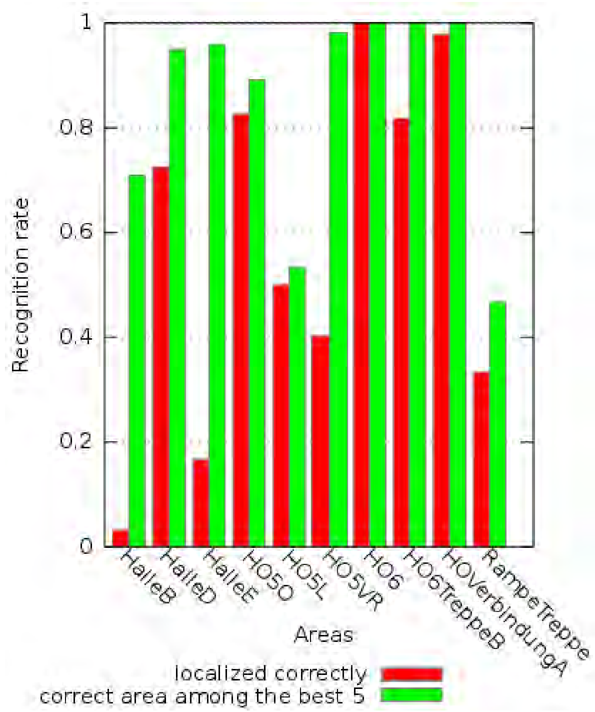

Figure 13: Example of the evaluation of 10 areas.

Sunlight
The strong sunlight and the reflections in the area *HO5VR* reduces the number of good gradients of the HOG descriptors.

Bad representative reference images
The number of shots and their positions need to be adapted to the localization area. Areas with very near objects and altitude differences have to have more shots than a large hall. Otherwise small altitude changes already lead to incorrect localization's as is shown in the area *RampeTreppe*.

Considering these limitation our approach achieved very good localization results. The areas *HO5O*, *HO6*, *HO6TreppeB* and *HOVerbindungA* are examples of the good performance of the HOG localization.

1.5.4 Localization performance

The speed of the HOG localization is given by an example with an image size of 1280 x 1024 pixels and a descriptor database with 175 reference images. The descriptor calculation needs 0.1942s using an Intel Xeon E3-1231V3 (comparable to Intel i7-4770). The comparison of the descriptors with all database descriptors needed 0.0041 seconds on average. After the sum of both periods we have a localization result.

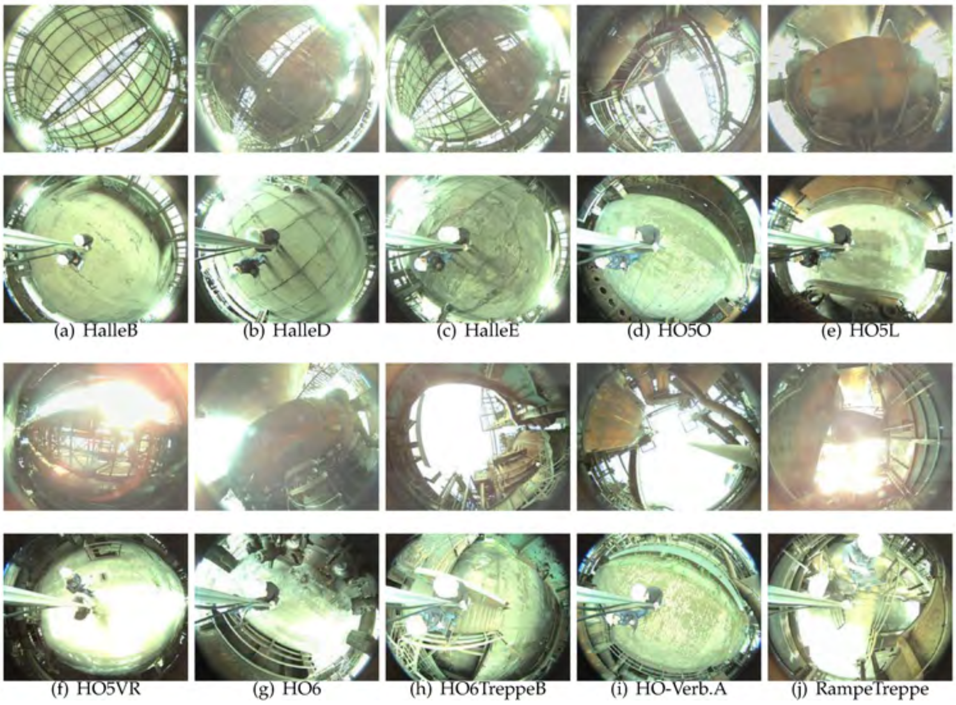

Figure 14: Example of 10 of the 33 localization areas. An upper and lower images define a comparison images (a - j) for the descriptor calculation.

1.5.5 HOG localization conclusion

In the last period we developed a localization method for two omnidirectional cameras on an unmanned aerial vehicle and tested it under real conditions. First, we selected a UAV suitable omnidirectional camera system. Second, we used a global appearance method based on HOG descriptors ([22, 24]) and showed that it is suitable for the UAV localization. Third, we tested the approach at the disused blast furnace plant Phoenix West at Dortmund-Hörde (Germany). Our results show that a localization based on global-appearance descriptors is fast and reliable.

1.5.6 Low-Level Navigation and UAV optimization

For the described UAV navigation, a robust low level control is necessary. This control layer is supposed to stabilize the UAV locally so that all high level control loops can rely on this inner loop without the need of being completely real-time. In D2.1 we described this inner loop running at a high control frequency of 500-1000 Hz and including a low level position control and obstacle avoidance system. To do so, in Year 1 we evaluated Stereo Vision, Structured Light, Ultrasonic and Lidar with very simple but robust algorithms. This analysis and ASC‘s cooperation with Intel led to

Figure 15: AscTec Firefly with an early Version of the RealSense™Sensor Ring

the decision of using Intel®RealSense™Technology. These very lightweight camera modules combine stereo vision and structured light and contain on-chip vision processing outputting 3D point clouds. In order to have nearly complete 360 degree vision, six of these modules with a field of view of 56 degree horizontal and 46 degree vertical were combined in a sensor ring. Figure 15 shows an early prototype developed in cooperation with Intel and presented at CES 2015.

Further work was done evaluating RealSense in various light conditions. Not surprising, the system was working great as long as either the stereo vision or the structured light is working well. The following critical situations were detected:

1. White walls and sunlight outdoor: In bright sunlight conditions, the structured light has nearly no effect. Therefore the system needs to rely on stereo vision, not working in front of texture free surfaces.

2. Glass and mirrors are not detected.

3. Black nets or surfaces absorbing IR structured or ambient light are only detected at the edges.

4. Very thin structures are detected only from a closer distance.

5. Objects out of range: A robust range of 8 m was determined during the experiments. Above the noise increases significantly. However data of up to 15 m distance can be used e.g. to limit the maximum speed.

To overcome these difficulties and in order to create a system being robust in most situations we aim for a combination of RealSense and very lightweight ultrasonic sensors. The hardware of the ultrasonic sensors is already integrated in the most recent setup while the software integration is

Figure 16: AscTec Neo with RealSense$^{\mathrm{TM}}$and ultrasonic sensors shown at IROS

future work for Year 3. Figure 16 and 17 shows the combined RealSense and Ultrasonic sensor setup mounted on an early prototype of the AscTec NEO, modified for TRADR and shown at IROS in Hamburg 2015.

Hardware Setup

Although the RealSense camera performs a lot of computation internally a lot of data needs to be transmitted to a dedicated computer board. Subscribing to all available data leads to a data rate of 1Gbit/s. To receive and process this data, a new version of ASC‘s Atom Computer board was developed and integrated. The data transmission is done by USB 3 directly connected to specially designed PCI Express adapter boards. The Bay Trail class quad core Atom processor allows speeds of up to 1.93Ghz per core. Figure 18 shows one of these sensor setup including the cabling in a special designed carbon fibre housing.

Having all these high speed data connections and high computation demands in small space, electromagnetic radiation needs to be considered, especially when combining this sensor setup with a highly sensitive GPS receiver. The additional GPS is necessary because the RealSense only has limited range and in open spaces GPS needs to be included to provided waypoint following and position hold capabilities on the same vehicle. So far this could only be solved using additional copper shielding and increasing the distance between the RealSense Sensor Ring and the GPS receiver as shown in Figure 17.

Height control and Position hold in larger indoor environments

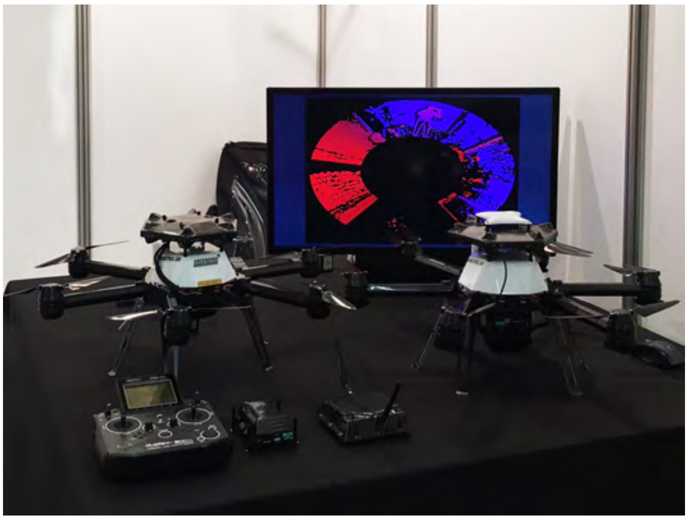

Figure 17: AscTec Neo with RealSense™and ultrasonic sensors shown at IROS; outputting the view of the sensors

Performing first tests in the Phoenix Site in Dortmund during T-JEX 2015 we noticed that an additional low level position hold system is necessary in larger indoor areas, because no GPS is available and the vehicle could easily be flying at a distance from walls or obstacles exceeding the robust range of the RealSense cameras. This results in drifting of the UAV until it reaches a position close to obstacles. Furthermore a precise height measurement is necessary for indoor flight to overcome the drift and inaccuracy of air pressure based height control. To solve both issues, a combined payload of an optical flow sensor and laser height sensor was integrated and shown for the first time at IROS in Hamburg. Figure 16 shows this sensor module with and without housing.

Software integration

Since the coverage of the Realsense sensor ring is 360deg in the horizontal plane it is possible to use the distance information around the AscTec Neo to compute and integrate a relative position even in GPS denied environments. The down looking obstacle flow sensor can additionally support indoor flights. In both indoor and outdoor environments, the data is used to create a virtual force field around obstacles which are added to the current horizontal speed commands. This is the basic virtual safety bumper which ensures that the UAV doesn't hit an obstacle. In order to allow more dynamic flight through several obstacles, a local path planner determines the best path that is free of obstacles and moves in the desired direction. The parameters of the path planning are set so that the path avoids the virtual

Figure 18: RealSense^{TM}sensor ring: onboard CPU and cabling

force field described above. Using this two-layered approach in combination with a robust position and speed estimation through GPS or self localization, a dynamic but still safe behaviour is achieved.

UAV optimization and use during the Joint events

For all UAV related work in TRADR, ASC's new flight control Trinity, providing full redundancy and a user programmable 168 MHz STM 32 processor, is to be used. To facilitate the transition, a Falcon 8 UAV, upgraded with the new Trinity flight control, was used for T-JEX and T-EVAL in 2015. For research related work, early versions of the new Asctec Neo, based on the EuRoC project, were used and modified with bigger motors in order to increase payload and endurance. Figures 19 and 20 shows different payload and battery setups with the original 9 inch propellers compared to the enlarged 11 inch version. This vehicle is further described in D6.2, and will be the main TRADR UAV. All work done in parallel on the Falcon UAV can easily be ported to the NEO because both UAVs now share the same flight control system.

1.6 Relation to the state-of-the-art

In this section we will describe how the results of D2.2 relate to the state-of-the-art.

1.6.1 Intelligent Teloperation of UGVs.

To address the UGV teleoperation and situational awareness problem described in Section 1.3 above, a lot of work has been devoted to the design of

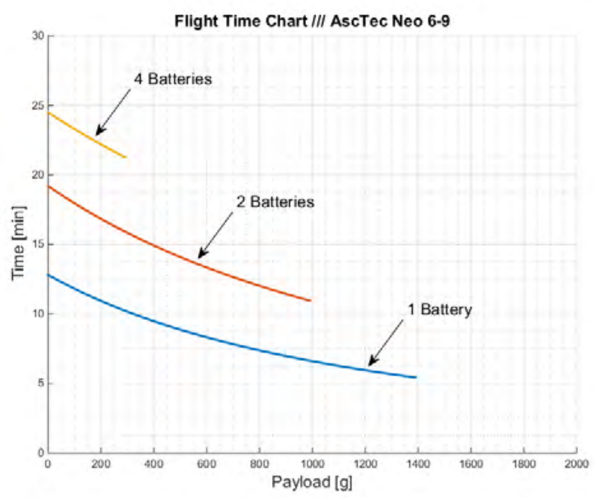

Figure 19: Flight Time Payload Diagramm for the 9 inch version

Operator Control Units (OCUs).

In a study of OCUs based on experiences from the AAAI Robot Rescue Competitions in 2002-2004 [25], the authors noticed an evolution over time, towards a large single interface, with a large percentage of the screen dedicated to video. The idea of creating a virtual 3D rendering of the UGV and its surroundings was explored in [26] and the use of multi-touch OCUs including fusion of sensor information to lower the operator's cognitive load was investigated in [27].

The issue of whether or not to use a pan tilt mounted camera on teleoperated UGVs was discussed in [9]. There, it was noted that so-called Travel-gaze decoupling makes a certain amount of ecological sense, since humans can easily look to the side while we move forward. However, it was concluded that: "This is probably too difficult to implement and the added degrees of freedom probably add to the complexity of the user's control problem". However, as we shall see Travel-gaze decoupling is not a problem when using FLC.

The idea of teleoperating a UGV using a First Person Shooter (FPS) interface was first suggested in [10]. There, the authors note that: "Urban Search and Rescue possesses most of the same characteristics as a successful computer game, ... and ... the FPS interface is most appropriate. It gives the user the most intuitive feel for the robot's situation, optimizing the decision-making ability of the operator. Per unit of robot time, this is, arguably, the most effective method of solving the task." The proposed solution is very related to the design presented here. It is argued that the User Interface (UI) should be composed of a large central video feed, with status updates in the form of icons in the periphery of the screen. The changes in status

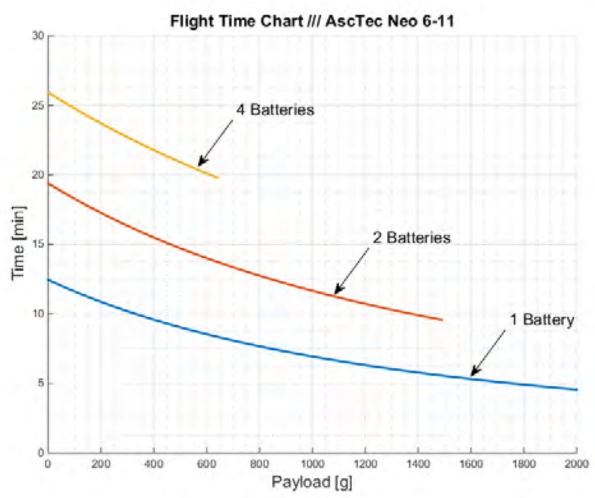

Figure 20: Flight Time Payload Diagramm for the 11 inch version

can then be examined in detail when the need arises, whereas large changes can be identified while still keeping eyes on the video feed. However, the authors are not able to fully implement the FPS interface, as can be seen in the following quote: "Unfortunately, *mouselook*, where moving the mouse rotates the player's head in the game world, was not something that could be implemented with the robot's existing PTZ camera implementation." Thus, the design in [10] was only able to implement a coarse approximation of the FPS interface, whereas our is exact.

The idea of exploring video games for new HRI interfaces was also discussed in [8]. There, it is argued that Video Game Based Frameworks (VGBF) are very useful for both evaluating existing OCUs and inspiring the design of new OCUs. The authors then go on to make a detailed categorization of input and output devices as well as methods used in different games and discuss different combinations of real video streams and rendered images of the vehicle surroundings.

In this paper, we go beyond the work described in [10], by investigating a version of FLC that is mathematically exact and verified in a prototype implementation.

1.6.2 Planning with dynamic maps

Classic planning techniques are often not suitable for use with dynamic maps as required in TRADR. Their most common drawback is the necessity to frequently re-plan when changes in the map occur. For the dynamics considered in TRADR and also intended by the graph-SLAM paradigm, frequent re-planning can quickly become time-consuming.

As the present planning approach serves as an intermediate solution, by not yet exploiting the graph-structure of the pose-graph, a look at the state-of-the-art shows promising avenues for the planning on dynamic pose-graph based maps.

[28] introduce an algorithm to plan under robot state uncertainty. Their method characterizes the a priori probability distribution of the robot state. This enables the optimization of the path accordingly.

[29] extend the approach further. They address three major limitations in planning under uncertainty: discretization of the state space, assumption of static environments and maximum likelihood observations by jointly optimizing paths for noise on robot and world states. The approach works on an inner and outer layer. The inner layer optimizes local paths and the outer layer optimizes global paths, therewith suitable for planning on pose-graph maps with local sub-maps and a globally connected graph.

[30] present an approach to locally repair a search-graph if changes in a map occur, in contrast to replanning for the whole track. Their approach is sampling based and aims to locally re-sample around map-changes to repair the planning tree.

[31] deal with the problem of high uncertainty in pose-graph maps by planning paths that favour nodes with low uncertainty. Their reasoning is that low node uncertainty results from more static environments around these nodes.

In conclusion, the state-of-the-art on planning under uncertainty clearly shows promising avenues, especially to limit planning times despite dynamic changes in the environment.

1.6.3 Mixed-initiative approaches for path planning

Semi-autonomous control allows for task sharing between a robot and an operator [32, 33, 34]. Under this setting, the robot focuses on low level tasks, such as terrain traversing, whereas the human operator is in charge of high-level control and supervisory tasks [35, 36, 37].

An interesting approach to semi-autonomous control with dynamic adjustment of the level of autonomy of the robot has been described in [35, 38]. In this approach, the control system is responsible of coordinating the interventions of the human operator and the low level robot activities, under a mixed-initiative planning setting.

[39, 40, 41] showed that the semi-autonomous control, under mixed-initiative, improves the performance of the robot, enhancing both the operator situation awareness and human-robot interaction.

TRADR inherits the main design principles underlying mixed-initiative approaches, to develop an alternative human-interaction model which also acts on the reasoning capabilities of the UGV platform. Human intervention does not only change the state of the execution of the robot task, but also the internal state of the robot perception where path planning takes place.

1.6.4 Learning patterns of motions of articulated tracked robots

Dynamic modeling is a key component of compliant and force control for complex robots, especially for actively articulated tracked robots [42]. However, due to unknown and hard to model non-linearities, analytic models of the dynamics for such systems are often only rough approximations. Nowadays, machine learning techniques are commonly applied to significantly improve model-based control [43]. In this regard, a number of methods have been proposed combining contextual policy search (CPS) [44] with prior knowledge [45] and regression [46, 47]. CPS is a popular means for multi-task reinforcement learning in robotic control [44]. CPS learns a hierarchical policy, in which the lower-level policy is often a domain-specific behavior representation such as dynamical movement primitives (DMPs) [48]. Learning takes place on the upper-level policy that defines a distribution over the parameters of the lower-level policy for a given context. This context encodes properties of the environment or the task. CPS is typically based on local search based approaches such as regression. Locally Weighted Projection Regression (LWPR), introduced in [49], is a local model which approximates non-linear mappings in high-dimensional space. Its computational complexity depends linearly on the amount of the training instances. A drawback of this approach is the large number of free parameters which are hard to optimize. In [45], the authors introduced prior knowledge in order to increase the generalization properties of LWPR. A large portion of the literature is focused on employing kernel-based methods for the estimation of the inverse dynamics mapping by employing approaches, such as Gaussian Process Regression (GPR) and Support Vector Regression (SVR) [50]. Local Gaussian Process (LGP), introduced in [46], handles the problem of real-time learning by building local models on similar inputs, based on a distance metric and uses the Cholesky decomposition for incrementally updating the kernel matrix. In [51], the authors propose a real-time algorithm, dubbed SSGPR, which incrementally updates the model using GPR as learning method. The model is capable of learning non-linear mappings by using random features mapping for kernel approximation, whose hyper-parameters are automatically updated. For the special case of relatively low-dimensional search spaces combined with an expensive cost function, which limits the number of evaluations of the cost functions, global search approaches, like Bayesian optimization are often superior, for instance for selecting hyper-parameters [52]. Bayesian optimization has been used for non-contextual policy search in robot grasping [53] and for locomotion tasks [54, 55]. The proposed approach for learning patterns of control manoeuvres for the TRADR UGV resorts to the main concepts underlying CPS. However, it differs from it by representing both the upper-level and the lower-level policies with a unified hierarchical model, defined by a Dirichlet Process-Gaussian Process (DP-GP) mixture model where the number of upper-level policies sufficient for describing robot motions is also learned from data. Gibbs sampling [56] and a hybrid Monte Carlo technique [57] are applied to obtain estimates of the concentration upper-level policies and of the the hyper-parameters of the lower-level policies, respectively. A similar approach has been used for modeling non-linear dynamics of moving targets [18, 19].

1.6.5 Localization of an unmanned aerial vehicle in GPS denied environments with a focus to optical cameras

Stereo camera systems and algorithms are well known for 3D perception of the environments [58]. Based on the left and right images, the stereo algorithms compute metrically correct 3D point clouds (in contrast to monocular structure from motion approaches). Variants of the ICP can be used to map the point clouds and / or to localize the base system. Schmid et. al [59] use the SGM algorithm at a FPGA to calculate point clouds in real time on board. Mapping is done in parallel to the point cloud calculation. Schmid et al. claimed to have the first autonomous flying robot with an on-board way point navigation and obstacle avoidance.

Monocular camera systems can also be used to generate 3D point clouds e.g. based on structure from motion techniques. Without additional sensor information, i.e. IMUs, structure from motion point clouds are not metrically correct. Nevertheless, they are often used since a camera is usually on-board to generate first person views. Only one example, Wang et al. [60], combine a monocular camera with a 2D laser scanner to estimate the states of an UAV (e.g. speed and position). Weiss et al. [61] present a monocular localization approach on the often used PTAM-algorithm [62] as well as Engel et al. (LSD SLAM) [63] and Forster et al. (SVO) [64].

Omnidirectional cameras are mono cameras with a wide field of view. Therefore, the pin hole camera model cannot be used. Camera calibration and distortion correction is more difficult, but the large field of view show more environment details e.g. to the drone pilot. Kim et al. [65] present an autonomous landing approach on a moving platform with omnidirectional cameras. The height and inclination are important information and computed based on the camera images [66].

1.6.6 Obstacle Avoidance

All described sensors and combinations of sensors are well known and described. But to our best knowledge, there is no other system combining several types of sensors as described in Section 1.5.6 above, in a truly lightweight and robust system. Compared to many other projects, it is very special in

TRADR that the results are not only shown in separated experiments in controlled environments. Instead, the system is to be used by end-users in a real scenario. Therefore the systems needs to be robust and lightweight, so that operational payloads like optical and thermal cameras can be added to the system. Most known other systems incorporate only a subset of sensors and have a high computational demand carrying heavy onboard computers reducing the payload capability for the real application.

2 Annexes

This section contains titles and abstracts of papers included in D2.2. Some of the papers are published, and some are not. The latter are not included in the public version of the deliverable.

2.1 (In Submission 2015), "Free Look UGV Control Tested in Game Environment: Enhanced Performance and Reduced Workload"

Bibliography Fredrik Båberg, Sergio Caccamo, Nanja Smets, Mark Neerincx, and Petter Ögren "Annexes for Dummies, a Non-Public Treatise." In Submission, December 2015.

Abstract Concurrent telecontrol of the chassis and camera of an Unmanned Ground Vehicle (UGV) is a demanding task for Urban Search and Rescue (USAR) teams. The standard way of controlling UGVs is called Tank Control (TC), but there is reason to believe that Free Look Control (FLC), a control mode used in games, could reduce this load substantially by decoupling, and providing separate controls for, camera translation and rotation. The general hypothesis is that FLC (1) reduces robot operatorsÕ workload and (2) enhances their performance for dynamic and time-critical USAR scenarios. A game-based environment was set-up to systematically compare FLC with TC in two typical search and rescue task: navigation and exploration. The results show that FLC improves mission performance in both exploration (search) and path following (navigation) scenarios. In the former, more objects were found, and in the later shorter navigation times were achieved. FLC also caused lower workload and stress levels in both scenarios, without inducing a significant difference in the number of collisions. Finally, FLC was preferred by 75 % of the subjects for exploration, and 56% for path following.

Relation to WP This paper is a core part of T2.2 Intelligent Teleoperation for UGVs.

Availability Restricted. Not included in the public version of this deliverable.

2.2 Caccamo (2015), "Extending a UGV Teleoperation FLC interface with Wireless Network Connectivity Information"

Bibliography Sergio Caccamo, Ramviyas Parasuraman, Fredrik Båberg, Petter Ögren. "Extending a UGV Teleoperation FLC interface with Wireless

Network Connectivity Information." In *Proceedings of the IEEE conference on Intelligent Robots and Systems (IROS '15)*, Hamburg, 2015.

Abstract Teleoperated Unmanned Ground Vehicles (UGVs) are expected to play an important role in future search and rescue operations. In such tasks, two factors are crucial for a successful mission completion: operator situational awareness and robust network connectivity between operator and UGV. In this paper, we address both these factors by extending a new Free Look Control (FLC) operator interface with a graphical representation of the Radio Signal Strength (RSS) gradient at the UGV location. We also provide a new way of estimating this gradient using multiple receivers with directional antennas. The proposed approach allows the operator to stay focused on the video stream providing the crucial situational awareness, while controlling the UGV to complete the mission without moving into areas with dangerously low wireless connectivity. The approach is implemented on a KUKA youBot using commercial-off-the-shelf components. We provide experimental results showing how the proposed RSS gradient estimation method performs better than a difference approximation using omnidirectional antennas and verify that it is indeed useful for predicting the RSS development along a UGV trajectory. We also evaluate the proposed combined approach in terms of accuracy, precision, sensitivity and specificity.

Relation to WP This paper is a core part of T2.2 Intelligent Teleoperation for UGVs.

Availability Unrestricted. Included in the public version of this deliverable.

2.3 Liebelt (2015), "3D Navigation for UAVs in GPS denied environments (master's thesis)"

Bibliography Tom-Marvin Liebelt. "UAV-Lokalisierung in Umgebungen ohne GPS-Empfang mithilfe von zwei omnidirektionalen RGB-Kameras." Master's thesis, Westphalian University of Applied Sciences Gelsenkirchen, August 2015.

Abstract The master thesis "UAV localization in GPS denied environments using two omnidirectional RGB cameras" is concerned with the localization of an unmanned aerial vehicle only with images from two omnidirectional cameras. It will present and explain the properties and possibilities of omnidirectional images. In the context of these thesis, a new localization method based on HOG descriptors was developed. This method is described

together with other global-appearance techniques. A comprehensive evaluation in a realistic environment is the conclusion of this work.

Relation to WP Within this thesis, a method for UAV localization has been developed, which was used in the context of T2.5.

2.4 Gianni (2015), "MIOM: a Mixed-initiative Operational Model for robots in Urban Search&Rescue"

Bibliography M. Gianni, F. Nardi, F. Ferri, F. Cantucci, M. A. Ruiz Garcia, K. Pushparaj and F. Pirri. "MIOM: a Mixed-initiative Operational Model for robots in Urban Search&Rescue." Accepted to the 18th International Conference on Control, Automation and Robotics (ICCAR'2016), December 2015.

Abstract In this paper we describe a Mixed-Initiative Operational Model (MIOM) which directly intervenes on the state of the functionalities embedded into a robot for Urban Search&Rescue (USAR) domain applications. MIOM extends the reasoning capabilities of the vehicle, i.e. mapping, path planning, visual perception and trajectory tracking, with operator knowledge. Especially in USAR scenarios, this coupled initiative has the main advantage of enhancing the overall performance of a rescue mission. Experiments with operators have been carried out to evaluate the effectiveness of this operational model.

Relation to WP This work is related to Task T2.5.

Availablity Restricted. Not included in the public version of this deliverable.

2.5 Gianni, Ruiz, Pirri(2015), "Learning the dynamics of Articulated Tracked Vehicles"

Bibliography M. Gianni, M. A. Ruiz Garcia F. Pirri. "Learning the dynamics of Articulated Tracked Vehicles". Accepted to the 18th International Conference on Control, Automation and Robotics (ICCAR'2016), December 2015.

Abstract In this work we propose a Bayesian non-parametric approach to modeling the motion control of ATVs. The motion control model is based on a Dirichlet Process-Gaussian Process (DPGP) mixture model. The DPGP mixture model provides a flexible representation of patterns of control manoeuvres along trajectories of different lengths and discretizations. The model also estimates the number of patterns, sufficient for modeling the dynamics of the ATV.

Relation to WP This work is related to Task T2.5.

Availablity Restricted. Not included in the public version of this deliverable.

Extending a UGV Teleoperation FLC Interface with Wireless Network Connectivity Information

Sergio Caccamo, Ramviyas Parasuraman, Fredrik Båberg, Petter Ögren

***Abstract*— Teleoperated Unmanned Ground Vehicles (UGVs) are expected to play an important role in future search and rescue operations. In such tasks, two factors are crucial for a successful mission completion: operator situational awareness and robust network connectivity between operator and UGV. In this paper, we address both these factors by extending a new Free Look Control (FLC) operator interface with a graphical representation of the Radio Signal Strength (RSS) gradient at the UGV location. We also provide a new way of estimating this gradient using multiple receivers with directional antennas. The proposed approach allows the operator to stay focused on the video stream providing the crucial situational awareness, while controlling the UGV to complete the mission without moving into areas with dangerously low wireless connectivity.**

The approach is implemented on a KUKA youBot using commercial-off-the-shelf components. We provide experimental results showing how the proposed RSS gradient estimation method performs better than a difference approximation using omnidirectional antennas and verify that it is indeed useful for predicting the RSS development along a UGV trajectory. We also evaluate the proposed combined approach in terms of accuracy, precision, sensitivity and specificity.

Fig. 1: A youBot mobile robot equipped with wireless network hardware used in the experiments. The directional antennas are visible in the corners of the youBot, and the omnidirectional antenna for communication in the center.

I. Introduction

Today, Unmanned Ground Vehicles (UGVs)[1] play an increasingly important role in several applications, such as Urban Search And Rescue (USAR), Explosive Ordinance Disposal (EOD), reconnaissance and inspections of disaster areas. In such missions, the operator needs robust wireless network connectivity not to loose control of the UGV, and a good situation awareness in order to decide what to do.

The importance of connectivity was made evident during a radiation survey mission at Fukushima, when the robot Quince was disconnected from the operator due to cable breakage, and was subsequently abandoned at the site [1]. Wireless channels are a natural alternative to cables, but present other challenges, such as shadowing or multipath fading, radio signal propagation effects that are difficult to predict, leading to low (or no) connectivity regions scattered throughout the environment [2], [3]. While increased autonomy in robots could solve some of the problems of low wireless connectivity [4], teleoperation of robots is still needed in many situations, since humans are still far more versatile than autonomous systems, especially in unknown and unpredictable environments [5], [6].

Another important aspect in USAR missions is the situational awareness. A number of studies have been addressing the subject, and it turns out that a significant amount of the UGV mission time is devoted to improving the operator situational awareness. In fact, the fraction of mission time spent on improving situational awareness was estimated to as much as 49% in [7] and to roughly 30% in [8]. Furthermore, [9] concluded that most of the critical incidents in the investigated USAR competition were due to lacking situation awareness. The challenge addressed in this paper is how to add the crucial awareness of network connectivity to the operator, without disturbing the normal (spatial) situational awareness. We do this by combining the Free Look Control (FLC) interface proposed in [10] with ideas regarding wireless information from [11], [12], and validate the approach using the UGV in Figure 1.

FLC is an interface borrowed from the computer gaming community, where it is used in so-called First Person Shooter (FPS) games, such as Halo, Half-Life, and Call of Duty [13]. The interface allows the operator to ignore the orientation of the UGV chassis, and completely focus on commands for moving the UGV camera through the remote environment.

In this paper we continue to take inspiration from the gaming world, and now look at how the gamer is made aware

The authors are with the Computer Vision and Active Perception Lab., Centre for Autonomous Systems, School of Computer Science and Communication, Royal Institute of Technology (KTH), SE-100 44 Stockholm, Sweden. e-mail: {caccamo|ramviyas|fbaberg|petter}@kth.se

The authors gratefully acknowledge funding from the European Union's seventh framework program (FP7), under grant agreement FP7-ICT-609763 TRADR.

[1]We will use the terms UGV and robot interchangeably in this paper.

of something happening around him/her. If a game character is hurt from behind, the bottom part of a circle surrounding the center of the screen flashes red. Similarly, if the character is hurt from the right side, the right part of the circle flashes red. Using similar ideas, we extend the FLC interface with a colored frame surrounding the camera view. The undesirable motion direction, from a network connectivity point of view, is now shown by coloring the corresponding part of the frame red. This is combined with a tactile vibration feedback when the threshold is close to being reached. We believe that this approach of combining more abstract signal strength gradient information with spatial situational awareness will work as well for UGV teleoperation, as it has done regarding changes in health level in the world of computer games.

The approach described above goes beyond the standard way of presenting the Radio Signal Strength (RSS), which is a signal strength indicator of the same type as the ones used to convey network status or battery level in most mobile phones today. To enable the new interface, we also need a reliable estimate of the gradient of the RSS, which provides the Direction of Arrival (DoA) information. This is done using a new hardware configuration, inspired by [11], [12], shown in Figure 1.

The main contributions of this paper can be summarized as:

1) we propose a new way of estimating RSS gradients using receiver spatial diversity with directional antennas;
2) we propose an extension of the FLC interface to include the RSS gradient estimates, enabling the operator to improve his situational awareness.

The outline of the paper is as follows. Section II presents the related work, followed by a description of the proposed methodology in Section III. Experiments validating the approach, performed indoor in both line-of-sight (LOS) and non line-of-sight (NLOS) conditions are detailed in Section IV. The results are presented in Section V and finally conclusions and future work are discussed in Section VI.

II. Related Work

Today, almost all teleoperated UGVs are equipped with cameras transmitting the live video feed to the operators Human Machine Interface (HMI) at a remote control station. A lot of work has been devoted to the HMI design to increase the situational awareness. For instance, in a study of operator control units based on experiences from the AAAI Robot Rescue Competitions in 2002-2004 [14], the authors noticed an evolution over time, towards a large single interface, with a large percentage of the screen dedicated to video.

A study conducted using response robots after the World Trade Center disaster has shown why it is essential to have a robust and stable wireless connection between the robot and the operator [2]. While some studies promote alternative and hybrid communication strategies [15], [16], [17], [12], there has been a very limited amount of research done in presenting the wireless connectivity information to the operator in an intuitive manner. In [11], a haptic device was used to provide feedback on wireless signal strength surrounding the robot. However, the HMI does not always include a haptic feedback device and hence using the visual interface is worth considering. To the best of our knowledge, this has not yet been explored in the literature.

The use of RSS gradients in radio source seeking or source localization has shown promising results in [12], [18], [19]. Measuring the RSS around the robot helps in estimating the RSS gradients which provide the DoA of radio signals at the robot location. There are several methods to estimate the RSS gradients, such as rotating directional antennas [20], [16], measurements at various positions in a specific manner [18], [19], and multiple receivers exploiting receiver diversity [12], [21]. Besides, it is shown in [21] that estimating the RSS gradients using receiver diversity outperforms antenna diversity approaches because of two reasons: low temporal influence in the RSS measurements and advantages such as reduced hardware complexity and energy needs (e.g. no rotating antennas), reduced overhead time in scanning for measurements, etc. In addition, [21] investigated various receiver placements on a robot for determining the RSS gradients and it is reported that the receivers (or antennas of receivers) placed on the corners of the robot resulted in better performance, and hence we retain this receiver configuration in this work.

In this paper, we propose a spatial-diversity method building upon the successful approaches used in [12], [11] to estimate the RSS gradients. However, we go beyond [12], [11] and apply directional antennas to each of the wireless receivers instead of omnidirectional antennas to increase the accuracy of the DoA estimation. Thus, the method proposed here (for the robot), and the active antenna tracking approach used in [16] (at the operator control station), are complementary ways of improving the end-to-end throughput of the wireless network. Furthermore, this paper transcends [10] by extending the FLC control mode with network connectivity information, and verifying that the DoA estimates does indeed give reliable information of the development of the RSS level.

III. Proposed Approach

In this section we present the proposed approach for improving operator situation awareness, including network connectivity awareness. First we describe the signal processing part (DoA estimation) of the approach. Then we describe the FLC control interface suggested in [10]. Finally, we describe the new HMI combining the above two components.

A. Radio signal strength DoA estimation

The Shannon-Hamilton theorem [22] states that the RSS received at a wireless receiver has direct impact on the network capacity (throughput) ($C \propto log(1 + 10^{(\frac{RSS-Noise}{10}})$), thereby permitting the RSS measure (in dB) as an indication of the network connectivity. The RSS can be modeled with the following equation:

$$RSS = RSS_{d_0} \underbrace{- 10\eta \log_{10}(\frac{d}{d_0})}_{deterministic} \underbrace{- \Psi(d) - \Omega(d,t)}_{stochastic}; \quad (1)$$

where RSS_{d_0} is the RSS at a reference distance (d_0), η is the propagation constant of the environment, d is the distance of the receiver from the radio source, Ψ is a stochastic (gaussian) variable representing (spatial) shadowing effects caused by the objects in the environment, and Ω is another stochastic variable in the RSS representing (spatial and temporal) multipath fading effects and dynamics in the environment [3]. The stochastic variations in the RSS can be mitigated by using a combination of filters and antenna diversity technique provided that the antenna spacing is far enough ($6\,\text{cm} \leq \Delta \leq 15\,\text{cm}$ for 2.4 GHz signal [3]) to experience uncorrelated fading. This fosters the use of RSS gradient-based approaches in robots.

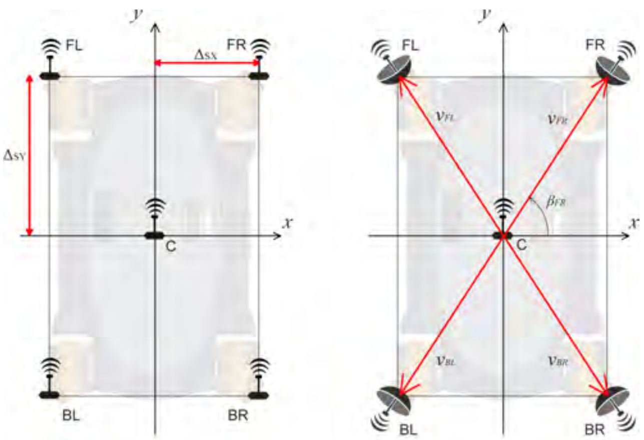

Fig. 2: Configuration of wireless adapters with (a) omnidirectional and (b) directional antennas surrounding the robot.

We propose the planar squared receiver configurations [21] in Figure 2 with either omnidirectional (left) or directional (right) antenna configurations. These configurations rely on the distances between antennas and on the differences between RSS magnitudes for obtaining RSS gradients. Modeling the RSS as a scalar field ($\Gamma(x) : \mathbb{R}^3 \to \mathbb{R}$), the above mentioned configurations permits to obtain an indirect estimation of the gradient (spatial derivative) of the RSS field. In the omnidirectional receivers configuration, the following finite difference formula [21] is applied on the RSS measurements from the Front-Right (FR), Front-Left (FL), Back-Right (BR), Back-Left (BL) receivers to obtain the RSS gradient vector $\overrightarrow{V_f} = [V_{f_x}, V_{f_y}]$, where

$$\begin{aligned} V_{f_x} &= \frac{(FR - FL)}{2\Delta_{SX}} + \frac{(BR - BL)}{2\Delta_{SX}}, \\ V_{f_y} &= \frac{(FR - BR)}{2\Delta_{SY}} + \frac{(FL - BL)}{2\Delta_{SY}}, \end{aligned} \quad (2)$$

and Δ_{sx}, Δ_{sy} are the spatial separation between antennas.

In the second configuration with directional antennas at the receivers, we use direct vector addition to obtain the DoA and use it as an RSS gradient estimate as follows:

$$\overrightarrow{V_f} = \widehat{V}_{FR} FR + \widehat{V}_{FL} FL + \widehat{V}_{BR} BR + \widehat{V}_{BL} BL \quad (3)$$

where $\widehat{V}_{FR}, \widehat{V}_{FL}, \widehat{V}_{BR}$ and $\widehat{V}_{BL}$ are unit vectors in the directions of the different sensors from the center of the UGV, as shown in Figure 2. This configuration relies on a weighted sum of vectors whose magnitudes are amplified by the RSS measurements from the respective receivers. Each antenna is oriented in the direction of its correspondent placement vector. Note that we are only interested in the direction of the estimate, not the magnitude. Thus we disregard the fact that the two estimates above have different magnitudes (and units).

Although we apply equation (3) in the second configuration, the finite difference method in equation (2) can also be used to estimate the RSS gradients as shown in [17]. Therefore it is possible to employ redundant schemes for computing RSS gradients so that device failures or misreadings can be tolerated to some extent (as discussed in [12]). Proving this fault-tolerance ability is beyond the scope of this paper, but will be included in future works.

The DoA of the radio signal is obtained from the RSS gradients as,

$$\text{DoA} = \tan^{-1}(\frac{V_{f_y}}{V_{f_x}}). \quad (4)$$

The two configurations share a common central point constituted by a central receiver with an omnidirectional antenna. The communication with the radio transmitter (source), which host the controller station, goes through the central receiver whereas the others receivers, even though connected to the radio source, are passive and only used for the RSS gradient estimation in this paper. We conduct experiments to verify the best configuration among the above two in Section IV.

B. *Free Look Control (FLC)*

In this section, we will describe the new FLC control mode, and compare it to Tank Control (TC), the control mode used in most UGVs today [10]. In TC, camera and robot platform controls are decoupled, requiring the user to mentally keep track of at least two angles while teleoperating an UGV: the camera angle relative to the UGV, and the platform orientation with respect to the world frame. In contrast, FLC couples both camera and platform control (while decoupling the orientation and translation) and thereby only requires the user to choose the desired direction of camera movement [10]. This makes FLC the most suitable control modality for the connectivity aware method we propose in this paper.

As in FPS video games, FLC commands are interpreted in relation to the camera view, moving forward means moving in the direction the camera is facing etc. A mathematical description of the FLC mode is provided below. We first define the kinematic movement of a general differential drive

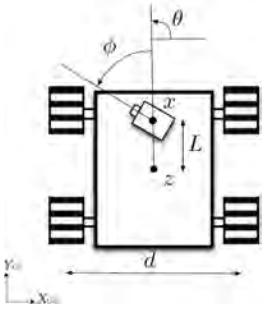

Fig. 3: A general differential drive robot mounted with a camera.

robot, see Figure 3, as in Equation (5) below.

$$\begin{aligned}\dot{z}_1 &= \frac{v_r + v_l}{2}\cos\theta,\\ \dot{z}_2 &= \frac{v_r + v_l}{2}\sin\theta,\\ \dot{\theta} &= \frac{v_r - v_l}{d},\\ \dot{\phi} &= k,\end{aligned} \tag{5}$$

where $z = (z_1, z_2)$ and $x = (x_1, x_2)$ are respectively the positions of the robot and camera in the global frame (GF), θ and ϕ are the orientations of the robot (in the GF) and the camera (relative to the robot), v_r, v_l are velocities of the right and left wheels/tracks respectively, d is the width of the vehicle, L is the distance between the camera center and the robot center, and k is the angular velocity of the camera relative to the robot. Note that the youBot in Figure 1 is not differential drive, but many search and rescue robots are, thus we treat that case here, and let the youBot emulate such a case.

Remember that the objective of the FLC mode is to combine the control of platform and the camera in such a way that the orientation and translation inputs are separated. This means that the resulting FLC kinematics should resemble the FPS control shown in Equation (6) (in our case, the camera corresponds to the FPS character).

$$\begin{aligned}\begin{pmatrix}\dot{x}_1\\ \dot{x}_2\end{pmatrix} &= \begin{pmatrix}\cos\psi & -\sin\psi\\ \sin\psi & \cos\psi\end{pmatrix}\begin{pmatrix}v_x\\ v_y\end{pmatrix},\\ \dot{\psi} &= \omega,\end{aligned} \tag{6}$$

where (x_1, x_2) and $\psi = \theta + \phi$ are position and orientation of the camera (FPS character), v_x and v_y are the inputs from the gamepad, to represent front/back and left/right motions respectively, and ω is the orientation input to the camera provided from the gamepad.

This conversion (from Equation (5) to Equation (6)) is realized by applying a control model shown in Equation (7) that maps the user inputs (v_x, v_y, ω) to the kinematic inputs (v_r, v_l, k). More detailed description and proofs are in [10].

$$\begin{aligned}\begin{pmatrix}v_l\\ v_r\end{pmatrix} &= \begin{pmatrix}1/2 & 1/2\\ -L/d & L/d\end{pmatrix}^{-1}\begin{pmatrix}\cos\phi & -\sin\phi\\ \sin\phi & \cos\phi\end{pmatrix}\begin{pmatrix}v_x\\ v_y\end{pmatrix},\\ k &= \omega - \frac{v_r - v_l}{d},\end{aligned} \tag{7}$$

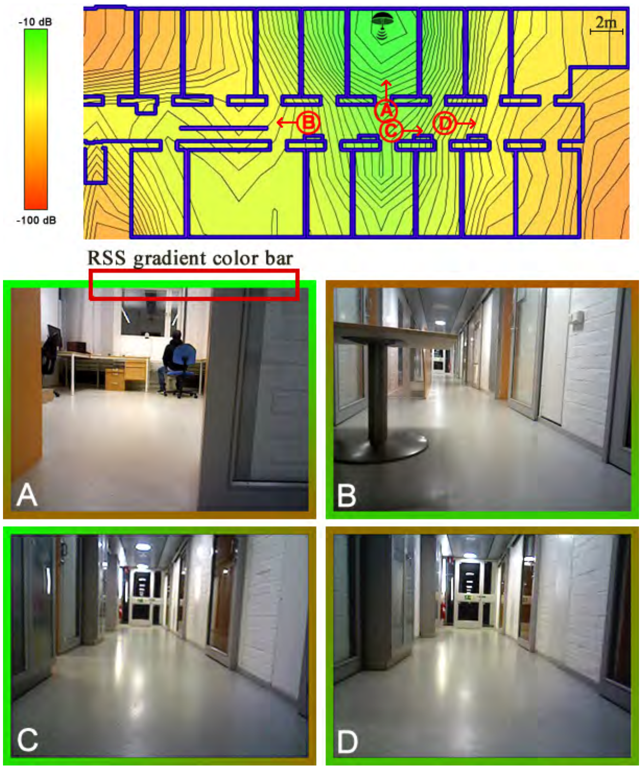

Fig. 4: Visualization of the RSS heat-map along with the robot locations and the view of the developed interface (HMI) at example positions (A-D). Arrows from A-D represents the camera's orientation. Note the green and red gradient, indicating higher and lower signal directions in the color bars surrounding the videos.

C. User Interface (HMI)

In a way that is similar to the way video games are controlled today, the operator HMI consists of a visual interface (monitor) providing a video feed from the robot during robot teleoperation. To provide visual feedback regarding the estimated DoA, we propose to use a rectangular border around the video feed, as illustrated in Fig 4.

The DoA estimates from Equation (4) are first mapped to the camera frame (by using the robot and camera orientations, and the FLC logic) and then translated to a color gradient, where a green color in the color bar indicates the higher signal strength direction, whereas a red color indicates a lower signal strength direction. Besides, the color intensity is scaled according to a linear interpolation of the measured RSS values. Thus the interface not only represents DoA but also gives a sense of the true RSS.

The code for estimating the DoA, generating the visual feedback, and also for the control mode, runs on the operator station, hence it does not increase the computational effort onboard the robot.

IV. Experimental evaluation

To verify the proposed approach, we performed two different experiments. The first experiment compares the accuracy of the DoA using the proposed directional antennas configuration with the omnidirectional configuration. The second experiment investigates the usefulness of the proposed approach by verifying that the variation of the RSS along a robot path is indeed predicted by the DoA estimates.

A. Experimental setup

1) Hardware: For the experiments, we used a KUKA youBot equipped with an arm as shown in Figure 1. The video feed is provided by a PrimeSense camera, attached to the robot arm which acts as a pan-tilt system for the camera. A commercial Wi-Fi access point (AP) with a detachable external antenna is used as the radio signal source (transmitter). Five small USB wireless adapters of the same model (TP-Link TL-WN722N) with detachable external antennas are attached to the robot. These wireless adapters (WiFi stations) act as the radio receivers and are connected to the AP using the IEEE 802.11n 2.4 GHz channels. All connections are optimized for channel interference based on adjacent channels and unwanted networks in the environment.

Four wireless adapters (used for DoA estimate) connected to directional dish antennas ($8\,\mathrm{dBi}$) are placed at the robot's vertices as can be seen in Figures 1 and 2b. Here, the sensors' spatial separations are $\Delta_{SX} = 0.4m, \Delta_{SY} = 0.6m$. A fifth adapter (used for communication with the operator) is placed at the center and is connected to an external omnidirectional whip antenna ($4\,\mathrm{dBi}$).

For comparison with the DoA estimate using omnidirectional antenna configuration, we replaced the directional antennas with (external) omnidirectional whip antennas ($4\,\mathrm{dBi}$) and placed them on the robot as depicted in Figure 2a with $\Delta_{SX} = 0.4m, \Delta_{SY} = 0.4m$. In addition, we conducted the experiments with either omnidirectional whip ($8\,\mathrm{dBi}$) or directional dish ($8\,\mathrm{dBi}$) antennas at the AP with the transmit power fixed at $20\,\mathrm{dBm}$. All the external antennas costed less than \$10 each.

2) Environment: It is well known that indoor environments are more challenging for wireless systems, in terms of e.g. multipath fading phenomena. Therefore we chose an office environment ($400\,\mathrm{m}^2$), including a hallway and a set of rooms, to perform our experiments. To get an overview of the RSS variations in the environment, we generated a heat-map of the RSS with fine measurements using a commercial wireless survey tool[2]. The floor map along with the RSS heat-map is shown in the upper part of Figure 4. The hallway has $47\,\mathrm{cm}$ thick concrete walls, while the walls in between offices are thinner and made of glass and plaster.

3) Signal processing and HMI: The FLC and the signal processing on the RSS are implemented in the Robot Operating System (ROS) framework. A laptop running Ubuntu 14.04, with a connected Xbox gamepad, is used for the teleoperation experiments. The laptop acts as the operator control station, provides the HMI to the operator and communicates with the robot through the wireless AP. The wireless adapters used in the study provide the RSS information using the Received Signal Strength Indicator (RSSI[3]) metric, directly in terms of dBm. The RSSI is sampled at $5\,\mathrm{Hz}$ rate. As the RSS measurements are noisy, we applied an exponential moving average filter using the following model [12]:

$$\widehat{RSS}_i = RSS_{i-1} + \alpha(RSS_i - RSS_{i-1}), \tag{8}$$

to remove temporal fluctuations, where α is the smoothing parameter, set to 0.75 based on empirical tests. Following [23], we also applied a Moving Average Filter (MAF) to mitigate spatial multipath fading, with a window size equal to about 10λ (λ is the wavelength). For instance, at $0.2\,\mathrm{m/s}$ velocity, $5\,\mathrm{Hz}$ RSS sampling rate, and $\lambda = 12.5\,\mathrm{cm}$ (at $2.4\,\mathrm{GHz}$), the MAF window size should be ≈ 30 to filter samples within $1.25\,\mathrm{m}$ (10λ) displacement by the robot.

B. Experiments

1) Antenna configurations: The two configurations proposed in Section III-A are evaluated with both omnidirectional and directional antennas at the AP (transmitter) side, resulting in the following four combinations: Directional Tx (Transmitter) - Directional Rx (Receiver); Directional Tx - Omnidirectional Rx; Omnidirectional Tx - Directional Rx; and Omnidirectional Tx - Omnidirectional Rx. To evaluate which antenna configuration provides the best estimation of the DoA, we conducted several trials for each of the four configuration in LOS and NLOS conditions. The robot was placed at a fixed distance from the radio source and rotated following a pre-determined pattern, to ensure repeatability, with different velocities ($0.1, 0.2$ and $0.5\,\mathrm{rad/s}$) taking measurements as can be seen in Figure 5.

2) System evaluation: Once the more appropriate antenna configuration is chosen, we performed a set of experiments aimed to evaluate the sensitivity, specificity, accuracy and precision of the network connectivity feedback information provided by the interface. The robot is teleoperated (at a velocity $\leq 0.2\,\mathrm{m/s}$) for a random exploration task within the floor, simulating short missions, following different paths and trying to avoid low connectivity regions using the proposed interface. Eight different trials of this kind are conducted. In each trial, the transmitter is placed at different locations. An example trajectory made by the robot is shown in Figure 6. During each trial, we logged the robot odometry data (which is not very accurate as can be observed in Figure 6), the RSS data, the estimated DoA and the streamed video. A video illustrating the proposed method with an example trial is available[4].

In a noise free world the following equality would hold:

$$\frac{dRSS}{dt} = \frac{dRSS}{dx}\frac{dx}{dt}\ . \tag{9}$$

The real world is however far from noise free, and we must experimentally verify that our estimates provide useful information to the human operator. We foresee that if the

[2]Ekahau site survey tool.

[3]RSSI is a vendor-specific metric and therefore reports different values (or quantities) in different devices. The wireless adapters used in this paper reported reliable values of absolute signal power (dBm) as RSSI.

[4]https://youtu.be/YcbPi1c7eaQ

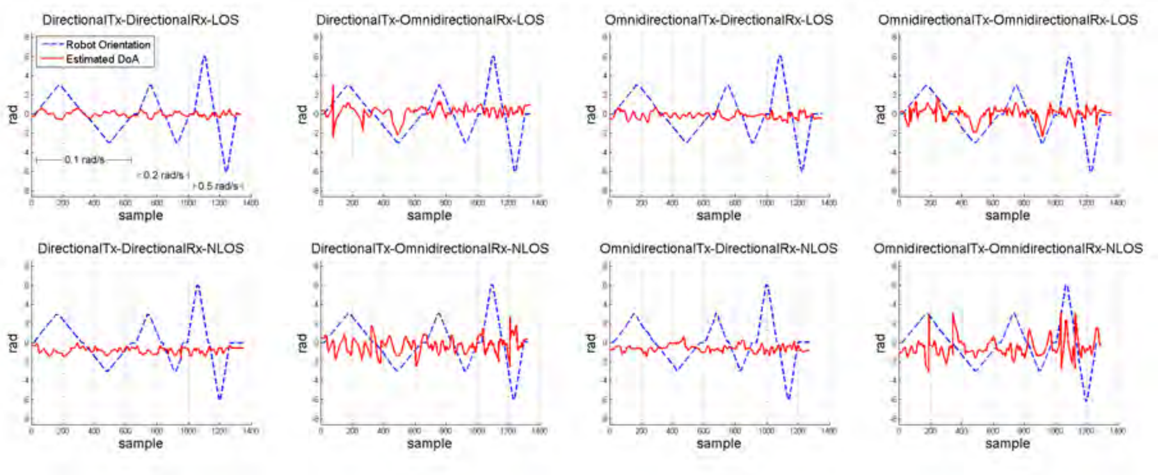

Fig. 5: DoA estimation results of the two configurations of receivers (shown in Figure 2) with directional transmitter (row 1) and omnidirectional transmitter (row 2). As can be seen, the use of directional receivers configuration (column 1 and 3) resulted in significantly less errors than omnidirectional receivers (column 2 and 4).

robot is moved in the direction of the estimated DoA, the measured RSS will increase. For this we used the RSS at

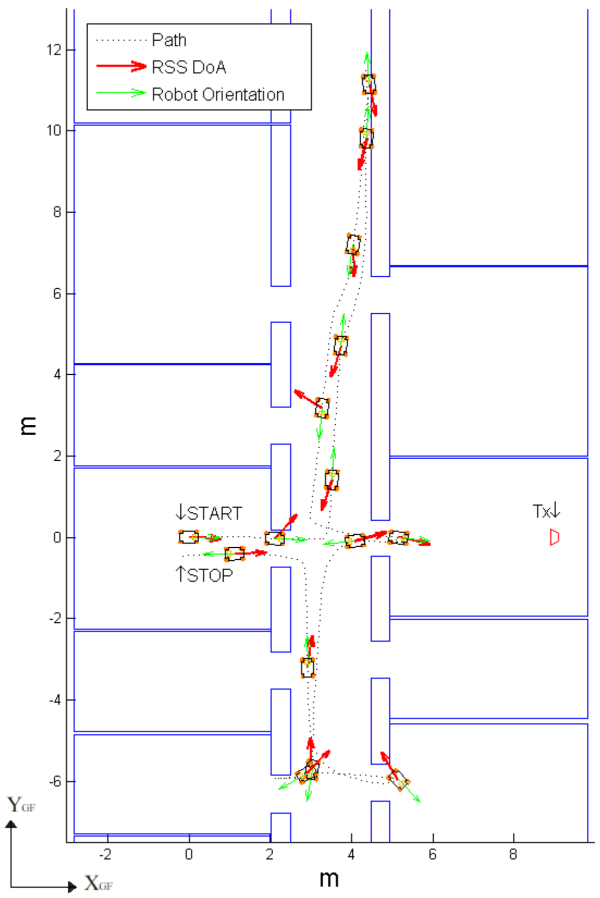

Fig. 6: Trajectory (downsampled) of the UGV in one of the experiments. The red arrows show the RSS DoA and the green arrows show the robot orientation in the global frame.

the central receiver to cross-verify the DoA obtained by the antennas on the vertices of the robot. We used finite differences in $\widehat{RSS_C}$ to estimate $\frac{dRSS}{dt}$, and $\overrightarrow{V_f}$ as the estimate of $\frac{dRSS}{dx}$ and the odometer robot velocity $\overrightarrow{V_{UGV}}(t)$ to estimate $\frac{dx}{dt}$. The scalar (dot) product between the robot velocity and the computed RSS gradient $\overrightarrow{V_f}$ at each instant is given by:

$$p(t) = \langle \overrightarrow{V_f}(t), \overrightarrow{V_{UGV}}(t) \rangle. \tag{10}$$

By comparing the scalar product $p(t)$ with the change in the RSS at the central receiver $\nabla_t RSS_C = \frac{dRSS_C}{dt}$, we can evaluate the proposed teleoperation system quantitatively. We expect a steep increase in RSS_C when $p(t)$ is positive and close to 1 (i.e. every time the user is moving towards the DoA). Similarly, we expect a sharp decrease in RSS_c when the p(t) is negative and close to -1 (i.e. the user moves the robot away from the DoA).

V. Results and Discussions

A. Antennas configurations

Figure 5 shows the results of the experiments with various antenna arrangements. Each plot shows the robot orientation (blue) and DoA of the RSS (red) in the global frame at each instant. We calculate the circular mean, $\bar{\phi} = atan2\left(\frac{\sum_{j=1}^{n} \sin\phi_j}{n}, \frac{\sum_{j=1}^{n} \cos\phi_j}{n}\right)$ and the circular standard deviation (STD) $= \sqrt{1 - \|\mathbf{r}\|}$, where $\mathbf{r} = \left[\frac{\sum_{j=1}^{n} \sin\phi_j}{n}, \frac{\sum_{j=1}^{n} \cos\phi_j}{n}\right]$. The reported angular mean, even though useful for comparison, does not account into the dynamics (temporal variations) of the DoA estimates, thereby the STD (or variance) predominates the analysis in this section. We expect the DoA to point toward the source (AP) or the highest RSS in the local region at every instant irrespective of the robot orientation.

Table I presents the results of the four antenna arrangements in a LOS condition. The expected DoA in these four cases is 0 rad (hence the estimated DoA also indicates the error in DoA estimation), which is the relative orientation

Transmitter	Receiver	Mean DoA (rad)	STD (rad)
Directional	Directional	0.02	0.19
Directional	Omnidirectional	0.26	0.41
Omnidirectional	Directional	-0.17	0.23
Omnidirectional	Omnidirectional	0.07	0.42

TABLE I: Transmitter placed in LOS. Expected DoA is 0 rad.

Transmitter	Receiver	Mean DoA (rad)	STD (rad)
Directional	Directional	-0.84	0.21
Directional	Omnidirectional	-0.34	0.52
Omnidirectional	Directional	-0.62	0.24
Omnidirectional	Omnidirectional	-0.70	0.56

TABLE II: Transmitter placed in NLOS. Expected DoA is ≈ -1 rad.

of the robot with respect to the source in the global frame. Table II reports the results for the NLOS condition, where the robot is fully blocked by a thick concrete wall in the hallway and is separated from the source with a distance of 6m with relative orientation of -1 rad.

In both LOS and NLOS, and for both directional and omnidirectional transmitter settings, the omnidirectional receivers configuration (column 2 and 4 of Figure 5) consistently provided noisy DoA estimates (with rapid variations around the mean value). In contrast, the directional receiver configurations (column 1 and 3 of Figure 5) exhibited lower variance (or STD) and better accuracy (mean error < 0.2 rad in LOS, < 0.4 rad in NLOS). This means that the directional receiver configuration (Figure 2b) produced reliable and stable DoA estimates at every instant, which is vital for a teleoperation system with DoA feedback. The results support the observations in [16] that the directional antennas are best suited for active tracking of the DoA.

Overall, the configuration "Directional Tx - Directional Rx" resulted in low variance with reasonably high accuracy. Hence we use this configuration for the next experiment to evaluate the whole teleoperation system with DoA feedback.

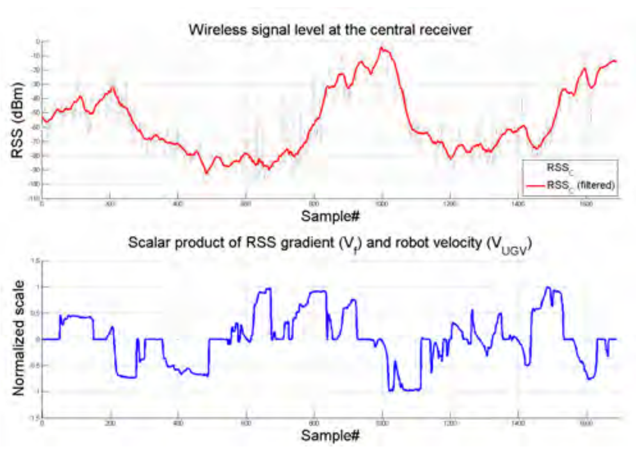

Fig. 7: Evaluation of the new UGV (robot) teleoperation FLC interface with wireless network connectivity perception.

B. System evaluation

Figure 7 shows the variations of RSS at the central receiver (RSS_C) and the scalar product $p(t)$ with time for the sample trial depicted in Figure 6. To quantify the system performances, we measure the number of true/false positives/negatives in the outcome. We define the *true positives* (TP) and *true negatives* (TN) as the number of occurrences where the user is driving in or away from the direction of the DoA while the RSS_C is increasing or decreasing respectively. Conversely, *false positives* (FP) and *false negatives* (FN) correspond respectively to the occurrences where the RSS_C is decreasing or increasing with the user's movement towards or away from the DoA. The following equations show how they are calculated.

$$TP = \sum_{t=1}^{N} H(\nabla_t RSS_C(t))H(p(t) - \tau), \tag{11}$$

$$FP = \sum_{t=1}^{N} H(-\nabla_t RSS_C(t))H(p(t) - \tau), \tag{12}$$

$$TN = \sum_{t=1}^{N} H(-\nabla_t RSS_C(t))H(-(p(t) - \tau)), \tag{13}$$

$$FN = \sum_{t=1}^{N} H(\nabla_t RSS_C(t))H(-(p(t) - \tau)), \tag{14}$$

where $\nabla_t RSS_C(t) = \frac{RSS_C(t+1) - RSS_C(t)}{T_s}$ with T_s being the RSS sampling interval, N is the number of samples analyzed, H is a unit step function (output is 0 for negative arguments and 1 for positive arguments), and τ is a threshold set to avoid zeros in the scalar product (explained later).

From these definitions, we compute Sensitivity ($\frac{TP}{TP+FN}$), Specificity ($\frac{TN}{FP+TN}$), Precision ($\frac{TP}{TP+FP}$), and Accuracy ($\frac{TP+TN}{TP+TN+FP+FN}$) metrics. The threshold value ($\tau \in \mathcal{R}^+$) is used to remove static measurements (where $p(t)$ is equal or close to 0) and to alleviate minute odometer errors such as a small linear velocity generated during a rotation in place (which empirically determines the value of τ).

It can be seen in Figure 6 that the estimated DoA sometimes pointed towards the corridor or the doorways (instead of the true source location). This is expected because of substantial exposure of radio signals from these regions. Table III shows the results obtained for the experiments conducted on different teleoperation missions as explained in the Section IV-B.2. The proposed system delivered 82%

Mission	Sensitivity	Specificity	Precision	Accuracy
1 (5.6 min)	0.87	0.79	0.78	0.83
2 (14.2 min)	0.70	0.85	0.82	0.77
3 (10.7 min	0.67	0.76	0.72	0.72
4 (10.0 min)	0.81	0.82	0.81	0.82
5 (11.1 min)	0.81	0.90	0.87	0.86
6 (11.4 min)	0.72	0.87	0.88	0.78
7 (5.0 min)	0.70	0.76	0.80	0.72
8 (5.5 min)	0.62	0.90	0.86	0.76
Mean	0.74	0.83	0.82	0.78

TABLE III: Evaluation of the system with sensitivity, specificity, precision and accuracy for different sorties, calculated with MAF window size = 30 and $\tau = 0.1$.

precision and 78% accuracy in guiding the teleoperator with network connectivity feedback in an indoor environment. As the analysis depend on the UGV's velocity from the odometer, we presume that odometry errors could have contributed to reduced accuracy of the proposed system. Thus a better localization technique will improve the overall system accuracy. The main limitations in the proposed solution are the physical constraints on the robot and reliability of the RSS readings. Note that the system is also reasonably sensitive (74%) in directing the operator into high wireless signal regions (towards DoA) while maintains high specificity (83%) in pointing out low-wireless signal regions.

Although the quantitative results presented in this paper are assuring, qualitative evaluation with user studies are nevertheless required to demonstrate the effectiveness of the new interface with human in the loop. This forms a basis of our future work. Additionally, the directional antennas used in this study can also be exploited for communication redundancy, offering advantages such as increased coverage, stable connections, and coverage in elevated regions [15].

VI. Conclusions

We looked at the possibility of providing a visually intuitive interface for presenting the network connectivity information with directionality at the HMI for naturally guiding the human operators to drive a mobile robot (UGV) into high wireless coverage regions and avoid low-wireless signal regions. We integrated this system with a novel Free Look Control (FLC) mode which provides a first person view of the surroundings from the robot camera, in a way that is similar to a First Person Shooter (FPS) computer game.

We proposed a spatial-diversity based technique with multiple directional wireless receivers to accurately estimate the radio signal strength (RSS) direction of arrival (DoA). We compared our proposed DoA estimation method with finite difference method using omnidirectional antennas and demonstrated that the DoA estimates using directional receivers resulted in high accuracy (mean error < 0.4 rad even in NLOS). Finally, we conducted experiments to objectively validate the proposed interface and have demonstrated high reliability and precision ($\approx 82\%$) in providing useful network connectivity information to the operator.

We believe that these results will provide a significant contribution towards creating a HMI where the operator situational awareness includes not only spatial components, but also network connectivity information, thus enabling better performance in time-critical robotic missions such as urban search and rescue.

References

[1] K. Nagatani, S. Kiribayashi, Y. Okada, S. Tadokoro, T. Nishimura, T. Yoshida, E. Koyanagi, and Y. Hada, "Redesign of rescue mobile robot Quince," in *IEEE International Symposium on Safety Security and Rescue Robotics*. IEEE, 2011, pp. 13–18.

[2] J. Casper and R. R. Murphy, "Human-robot interactions during the robot-assisted urban search and rescue response at the World Trade Center," *IEEE Transactions on Systems, Man and Cybernetics, Part B (Cybernetics)*, vol. 33, no. 3, pp. 367–385, 2003.

[3] M. Lindhè, K. H. Johansson, and A. Bicchi, "An experimental study of exploiting multipath fading for robot communications," in *Proceedings of Robotics: Science and Systems*, June 2007.

[4] A. Birk and H. Kenn, "A rescue robot control architecture ensuring safe semi-autonomous operation," *RoboCup 2002. Robot Soccer World Cup VI*, 2003.

[5] T. Fong and C. Thorpe, "Vehicle teleoperation interfaces," *Autonomous robots*, vol. 11, no. 1, pp. 9–18, 2001.

[6] R. Wegner and J. Anderson, "Agent-Based Support for Balancing Teleoperation and Autonomy in Urban Search and Rescue," *International Journal of Robotics and Automation*, vol. 21, no. 2, pp. 1–19, 2006.

[7] J. Burke, R. Murphy, M. Coovert, and D. Riddle, "Moonlight in Miami: An ethnographic study of human-robot interaction in USAR," *Human-Computer Interaction, special issue on Human-Robot Interaction*, vol. 19, pp. 1–2, 2004.

[8] H. Yanco and J. Drury, "Where Am I? Acquiring Situation Awareness Using a Remote Robot Platform," *IEEE Conference on Systems, Man and Cybernetics*, 2004.

[9] J. L. Drury, J. Scholtz, and H. A. Yanco, "Awareness in human-robot interactions," in *IEEE International Conference on Systems, Man and Cybernetics*, vol. 1. IEEE, 2003, pp. 912–918.

[10] P. Ögren, P. Svenmarck, P. Lif, M. Norberg, and N. E. Söderbäck, "Design and Implementation of a New Teleoperation Control Mode for Differential Drive UGVs," *Autonomous Robots*, 2014.

[11] A. Owen-Hill, R. Parasuraman, and M. Ferre, "Haptic teleoperation of mobile robots for augmentation of operator perception in environments with low-wireless signal," in *IEEE International Symposium on Safety, Security, and Rescue Robotics (SSRR)*, Oct. 2013.

[12] R. Parasuraman, T. Fabry, L. Molinari, K. Kershaw, M. D. Castro, A. Masi, and M. Ferre, "A Multi-Sensor RSS Spatial Sensing-Based Robust Stochastic Optimization Algorithm for Enhanced Wireless Tethering," *Sensors*, vol. 14, no. 12, pp. 23 970–24 003, 2014.

[13] K. Gkikas, "The evolution of FPS games controllers: how use progressively shaped their present design," in *Panhellenic Conference on Informatics (PCI)*, 2007.

[14] H. A. Yanco and J. L. Drury, "Rescuing interfaces: A multi-year study of human-robot interaction at the AAAI Robot Rescue Competition," *Autonomous Robots*, vol. 22, no. 4, pp. 333–352, 2007.

[15] Y. Hada and O. Takizawa, "Development of communication technology for search and rescue robots," *Journal of the National Institute of Information and Communications Technology*, vol. 58, no. 1, 2011.

[16] B.-C. Min, E. Matson, and B. Khaday, "Design of a networked robotic system capable of enhancing wireless communication capabilities," in *IEEE International Symposium on Safety, Security, and Rescue Robotics (SSRR)*, Oct 2013.

[17] N. Bezzo, B. Griffin, P. Cruz, J. Donahue, R. Fierro, and J. Wood, "A cooperative heterogeneous mobile wireless mechatronic system," *IEEE/ASME Transactions on Mechatronics*, vol. 19, no. 1, pp. 20–31, Feb. 2014.

[18] D. Han, D. Andersen, M. Kaminsky, K. Papagiannaki, and S. Seshan, "Access point localization using local signal strength gradient," in *Passive and Active Network Measurement*, ser. Lecture Notes in Computer Science, S. Moon, R. Teixeira, and S. Uhlig, Eds. Springer Berlin Heidelberg, 2009, vol. 5448, pp. 99–108.

[19] J. N. Twigg, J. R. Fink, P. Yu, and B. M. Sadler, "RSS gradient-assisted frontier exploration and radio source localization," in *IEEE International Conference on Robotics and Automation (ICRA)*. IEEE, 2012, pp. 889–895.

[20] S. Venkateswaran, J. T. Isaacs, B. M. Sadler, J. P. Hespanha, and U. Madhow, "RF source-seeking by a micro aerial vehicle using rotation-based angle of arrival estimates," in *Proc. of the 2013 Amer. Contr. Conf.*, June 2013.

[21] R. Parasuraman, T. Fabry, K. Kershaw, and M. Ferre, "Spatial sampling methods for improved communication for wireless relay robots," in *International Conference on Connected Vehicles and Expo (ICCVE)*. IEEE, Dec. 2013, pp. 874–880.

[22] C. Shannon, "Communication in the presence of noise," *Proceedings of the IRE*, vol. 37, pp. 10–21, 1949.

[23] R. Valenzuela, O. Landron, and D. Jacobs, "Estimating local mean signal strength of indoor multipath propagation," *IEEE Transactions on Vehicular Technology*, vol. 46, no. 1, pp. 203–212, Feb 1997.

References

[1] C. Lundberg, "Assessment and evaluation of Man-portable robots for High-risk professions in urban settings," Ph.D. dissertation, Royal Institute of Technology (KTH), Stockholm, Sweden, 2007.

[2] P. A. Buxbaum, "Robot Wars," *Defense Technology International*, March/April 2006.

[3] R. Murphy, "Human–Robot Interaction in Rescue Robotics," *IEEE Transactions on systems, Man, and Cybernetics, Part C: Application and Reviews*, vol. 34, no. 2, 2004.

[4] D. Woods, J. Tittle, M. Feil, and A. Roesler, "Envisioning Human–Robot Coordination in Future Operations," *IEEE Transactions on systems, Man, and Cybernetics, Part C: Application and Reviews*, vol. 34, no. 2, 2004.

[5] J. Burke, R. Murphy, M. Coovert, and D. Riddle, "Moonlight in Miami: An ethnographic study of human-robot interaction in USAR," *Human-Computer Interaction, special issue on Human-Robot Interaction*, vol. 19, pp. 1–2, 2004.

[6] H. Yanco and J. Drury, "Where Am I? Acquiring Situation Awareness Using a Remote Robot Platform," *IEEE Conference on Systems, Man and Cybernetics*, 2004.

[7] J. L. Drury, J. Scholtz, and H. A. Yanco, "Awareness in human-robot interactions," in *Systems, Man and Cybernetics, 2003. IEEE International Conference on*, vol. 1. IEEE, 2003, pp. 912–918.

[8] J. Richer and J. L. Drury, "A video game-based framework for analyzing human-robot interaction, characterizing interface design in real-time interactive multimedia applications," in *Proceedings of the 1st ACM SIGCHI/SIGART conference on human-robot interaction*. ACM, 2006, pp. 266–273.

[9] S. Hughes, J. Manojlovich, M. Lewis, and J. Gennari, "Camera control and decoupled motion for teleoperation," in *Systems, Man and Cybernetics, 2003. IEEE International Conference on*, Jan. 2003.

[10] B. A. Maxwell, N. Ward, and F. Heckel, "Game-based design of human-robot interfaces for urban search and rescue," in *In Computer-Human Interface Fringe*. Citeseer, 2004.

[11] K. Gkikas, "The evolution of FPS games controllers: how use progressively shaped their present design," in *Panhellenic Conference on Informatics (PCI)*, 2007.

[12] A. Cummings, "The Evolution of Game Controllers and Control Schemes and their Effect on their games," in *The 17th Annual University of Southhampton Multimedia Systems Conference*, 2007.

[13] M. Grimm, "No change coming to resident evil controls," in *The Escapist Magazine, March*, March 2009.

[14] M. Bosse, R. Zlot, and P. Flick, "Zebedee: Design of a spring-mounted 3-d range sensor with application to mobile mapping," *Robotics, IEEE Transactions on*, vol. 28, no. 5, pp. 1104–1119, 2012.

[15] P. Furgale, C. H. Tong, T. D. Barfoot, and G. Sibley, "Continuous-time batch trajectory estimation using temporal basis functions," *The International Journal of Robotics Research*, 2015. [Online]. Available: http://ijr.sagepub.com/content/early/2015/08/03/0278364915585860.abstract

[16] F. Ferri, M. Gianni, M. Menna, and F. Pirri, "Point cloud segmentation and 3d path planning for tracked vehicles in cluttered and dynamic environments," in *In Proceedings of the 3rd IROS Workshop on Robots in Clutter: Perception and Interaction in Clutter*, 2014.

[17] ——, "Point cloud segmentation and 3d path planning for tracked vehicles in cluttered and dynamic environments," in *In Proceedings of the 3rd IROS Workshop on Robots in Clutter: Perception and Interaction in Clutter*, 2014.

[18] J. Joseph, F. Doshi-Velez, A. S. Huang, and N. Roy, "A bayesian nonparametric approach to modeling motion patterns," *Autonomous Robots*, vol. 31, no. 4, pp. 383–400, 2011. [Online]. Available: http://dx.doi.org/10.1007/s10514-011-9248-x

[19] W. Wei, H.and Lu, P. Zhu, S. Ferrari, R. H. Klein, S. Omidshafiei, and J. P. How, "Camera control for learning nonlinear target dynamics via bayesian nonparametric dirichlet-process gaussian-process (dp-gp) models," in *IROS*, 2014, pp. 95–102.

[20] T.-M. Liebelt, "UAV-Lokalisierung in Umgebungen ohne GPS-Empfang mithilfe von zwei omnidirektionalen RGB-Kameras," Master's thesis, Westphalian University of Applied Sciences Gelsenkirchen, August 2015, http://publica.fraunhofer.de/dokumente/N-??????.html.

[21] D. Scaramuzza, A. Martinelli, and R. Siegwart, "A toolbox for easily calibrating omnidirectional cameras," in *Intelligent Robots and Systems, 2006 IEEE/RSJ International Conference on*, Oct 2006, pp. 5695–5701.

[22] N. Dalal and B. Triggs, "Histograms of oriented gradients for human detection," in *Computer Vision and Pattern Recognition, 2005. CVPR 2005. IEEE Computer Society Conference on*, vol. 1, June 2005, pp. 886–893 vol. 1.

[23] M. Hofmeister, M. Liebsch, and A. Zell, "Visual self-localization for small mobile robots with weighted gradient orientation histograms," in *IN: 40TH INTERNATIONAL SYMPOSIUM ON ROBOTICS (ISR*, 2009, pp. 87–91.

[24] L. PayÃą, F. AmorÃşs, L. FernÃąndez, and O. Reinoso, "Performance of global-appearance descriptors in map building and localization using omnidirectional vision," *Sensors*, vol. 14, no. 2, pp. 3033–3064, 2014. [Online]. Available: http://www.mdpi.com/1424-8220/14/2/3033

[25] H. A. Yanco and J. L. Drury, "Rescuing interfaces: A multi-year study of human-robot interaction at the aaai robot rescue competition," *Autonomous Robots*, vol. 22, no. 4, pp. 333–352, 2007.

[26] C. W. Nielsen, M. A. Goodrich, and R. W. Ricks, "Ecological interfaces for improving mobile robot teleoperation," *Robotics, IEEE Transactions on*, vol. 23, no. 5, pp. 927–941, 2007.

[27] M. Micire, J. L. Drury, B. Keyes, and H. A. Yanco, "Multi-touch interaction for robot control," in *Proceedings of the 14th international conference on Intelligent user interfaces.* ACM, 2009, pp. 425–428.

[28] J. van den Berg, P. Abbeel, and K. Goldberg, "LQG-MP: Optimized path planning for robots with motion uncertainty and imperfect state information," *The International Journal of Robotics Research*, vol. 30, no. 7, pp. 895–913, 2011.

[29] V. Indelman, L. Carlone, and F. Dellaert, "Planning Under Uncertainty in the Continuous Domain : a Generalized Belief Space Approach," in *IEEE International Conference on Robotics & Automation (ICRA)*, Hong Kong, 2014, pp. 6763–6770.

[30] M. Otte and E. Frazzoli, "RRTX: Asymptotically optimal single-query sampling-based motion planning with quick replanning," *The International Journal of Robotics Research*, 2015. [Online]. Available: http://ijr.sagepub.com/cgi/doi/10.1177/0278364915594679

[31] R. Valencia, M. Morta, J. Andrade-Cetto, and J. M. Porta, "Planning reliable paths with pose SLAM," *IEEE Transactions on Robotics*, vol. 29, no. 4, pp. 1050–1059, 2013.

[32] D. Bruemmer, R. Boring, D. Few, J. Marble, and M. Walton, “"i call shotgun!": an evaluation of mixed-initiative control for novice users of a search and rescue robot,” in *Systems, Man and Cybernetics, 2004 IEEE International Conference on*, vol. 3, 2004, pp. 2847–2852.

[33] R. Wegner and J. Anderson, “Agent-based support for balancing teleoperation and autonomy in urban search and rescue,” *Int. J. Robot. Autom.*, vol. 21, no. 2, pp. 120–128, 2006.

[34] B. Doroodgar, M. Ficocelli, B. Mobedi, and G. Nejat, “The search for survivors: Cooperative human-robot interaction in search and rescue environments using semi-autonomous robots,” in *ICRA*, 2010, pp. 2858–2863.

[35] A. Finzi and A. Orlandini, “Human-robot interaction through mixed-initiative planning for rescue and search rovers,” in *Proceedings of the 9th Conference on Advances in Artificial Intelligence*, ser. AI*IA’05. Berlin, Heidelberg: Springer-Verlag, 2005, pp. 483–494.

[36] Y. Okada, K. Nagatani, K. Yoshida, T. Yoshida, and E. Koyanagi, “Shared autonomy system for tracked vehicles to traverse rough terrain based on continuous three-dimensional terrain scanning,” in *IROS*, 2010, pp. 357–362.

[37] X. Perrin, R. Chavarriaga, F. Colas, R. Siegwart, and J. d. R. Millán, “Brain-coupled interaction for semi-autonomous navigation of an assistive robot,” *Robot. Auton. Syst.*, vol. 58, no. 12, pp. 1246–1255, 2010.

[38] A. Carbone, A. Finzi, A. Orlandini, and F. Pirri, “Model-based control architecture for attentive robots in rescue scenarios,” *Autonomous Robots*, vol. 24, no. 1, pp. 87–120, 2008.

[39] J. Drury, J. Scholtz, and H. Yanco, “Awareness in human-robot interactions,” in *Systems, Man and Cybernetics, 2003. IEEE International Conference on*, vol. 1, 2003, pp. 912–918.

[40] R. Murphy, “Trial by fire [rescue robots],” *Robotics Automation Magazine, IEEE*, vol. 11, no. 3, pp. 50–61, 2004.

[41] M. Baker, R. Casey, B. Keyes, and H. Yanco, “Improved interfaces for human-robot interaction in urban search and rescue,” in *Systems, Man and Cybernetics, 2004 IEEE International Conference on*, vol. 3, 2004, pp. 2960–2965.

[42] M. Gianni, F. Ferri, M. Menna, and F. Pirri, “Adaptive robust three-dimensional trajectory tracking for actively articulated tracked vehicles,” *Journal of Field Robotics*, pp. n/a–n/a, 2015. [Online]. Available: http://dx.doi.org/10.1002/rob.21584

[43] D. Nguyen-Tuong and J. Peters, "Model learning for robot control: a survey," *Cognitive Processing*, vol. 12, no. 4, pp. 319–340, 2011.

[44] M. P. Deisenroth, G. Neumann, and J. Peters, "A survey on policy search for robotics," *Foundations and TrendsÂő in Robotics*, vol. 2, no. 1âĂŞ2, pp. 1–142, 2011.

[45] J. S. Cruz, D. Kulić, and W. Owen, *Proceedings of the Second International Conference on Autonomous and Intelligent Systems*. Berlin, Heidelberg: Springer Berlin Heidelberg, 2011, ch. Online Incremental Learning of Inverse Dynamics Incorporating Prior Knowledge, pp. 167–176.

[46] D. Nguyen-Tuong, B. Scholkopf, and J. Peters, "Sparse online model learning for robot control with support vector regression," in *IROS*, 2009, pp. 3121–3126.

[47] J. de la Cruz, W. Owen, and D. Kulic, "Online learning of inverse dynamics via gaussian process regression," in *IROS*, 2012, pp. 3583–3590.

[48] A. J. Ijspeert, J. Nakanishi, H. Hoffmann, P. Pastor, and S. Schaal, "Dynamical movement primitives: Learning attractor models for motor behaviors," *Neural Comput.*, vol. 25, no. 2, pp. 328–373, 2013.

[49] S. Vijayakumar and S. Schaal, "Locally weighted projection regression: An o (n) algorithm for incremental real time learning in high dimensional space," in *ICML*, 2000.

[50] J. Kober, A. Wilhelm, E. Oztop, and J. Peters, "Reinforcement learning to adjust parametrized motor primitives to new situations," *Autonomous Robots*, vol. 33, no. 4, pp. 361–379, 2012.

[51] A. Gijsberts and G. Metta, "Real-time model learning using incremental sparse spectrum gaussian process regression," *Neural Networks*, vol. 41, pp. 59–69, 2013.

[52] J. Snoek, H. Larochelle, and R. P. Adams, "Practical bayesian optimization of machine learning algorithms," in *NIPS*, 2012.

[53] O. Kroemer, R. Detry, J. Piater, and J. Peters, "Combining active learning and reactive control for robot grasping," *Robotics and Autonomous Systems*, vol. 58, no. 9, pp. 1105–1116, 2010.

[54] D. J. Lizotte, T. Wang, M. H. Bowling, and D. Schuurmans, "Automatic gait optimization with gaussian process regression," in *IJCAI*, 2007.

[55] R. Calandra, N. Gopalan, A. Seyfarth, J. Peters, and M. P. Deisenroth, *Proceedings of the 8th International Conference on Learning and Intelligent Optimization.* Cham: Springer International Publishing, 2014, ch. Bayesian Gait Optimization for Bipedal Locomotion, pp. 274–290.

[56] C. E. Rasmussen and Z. Ghahramani, "Infinite mixtures of gaussian process experts," in *NIPS.* MIT Press, 2002, pp. 881–888.

[57] S. Duane, A. D. Kennedy, B. Pendleton, and D. Roweth, "Hybrid monte carlo," *Physics Letters B*, vol. 195, pp. 216–222, 1987.

[58] D. Scharstein and R. Szeliski. (2015) An evaluation of dense two-frame stereo algorithms. [Online]. Available: http://vision.middlebury.edu/stereo/

[59] K. Schmid, T. Tomic, F. Ruess, H. Hirschmuller, and M. Suppa, "Stereo vision based indoor/outdoor navigation for flying robots," in *Intelligent Robots and Systems (IROS), 2013 IEEE/RSJ International Conference on*, Nov 2013, pp. 3955–3962.

[60] F. Wang, J. Cui, S. K. Phang, B. M. Chen, and T. H. Lee, "A mono-camera and scanning laser range finder based uav indoor navigation system," in *Unmanned Aircraft Systems (ICUAS), 2013 International Conference on.* IEEE, 2013, pp. 694–701.

[61] S. Weiss, D. Scaramuzza, and R. Siegwart, "Monocular-slam–based navigation for autonomous micro helicopters in gps-denied environments," *Journal of Field Robotics*, vol. 28, no. 6, pp. 854–874, 2011.

[62] G. Klein and D. Murray, "Parallel tracking and mapping for small ar workspaces," in *Mixed and Augmented Reality, 2007. ISMAR 2007. 6th IEEE and ACM International Symposium on.* IEEE, 2007, pp. 225–234.

[63] J. Engel, T. Schöps, and D. Cremers, "LSD-SLAM: Large-scale direct monocular SLAM," in *European Conference on Computer Vision (ECCV)*, September 2014.

[64] C. Forster, M. Pizzoli, and D. Scaramuzza, "SVO: Fast semi-direct monocular visual odometry," in *IEEE International Conference on Robotics and Automation (ICRA)*, 2014.

[65] J. Kim, Y. Jung, D. Lee, and D. H. Shim, "Outdoor autonomous landing on a moving platform for quadrotors using an omnidirectional camera," in *Unmanned Aircraft Systems (ICUAS), 2014 International Conference on.* IEEE, 2014, pp. 1243–1252.

[66] A. Natraj, D. S. Ly, D. Eynard, C. Demonceaux, and P. Vasseur, "Omnidirectional vision for uav: Applications to attitude, motion and altitude estimation for day and night conditions," *Journal Of Intelligent & Robotic Systems*, vol. 69, no. 1-4, pp. 459–473, 2013.